


Targeting Discoidin Domain Receptors DDR1 and DDR2 overcomes matrix-mediated tumor cell adaptation and tolerance to BRAF-targeted therapy in melanoma

Ilona Berestjuk^{1,2}, Margaux Lecacheur^{1,2} , Alexandrine Carminati^{1,2}, Serena Diazzi^{1,2}, Christopher Rovera^{1,2}, Virginie Prod'homme^{1,2} , Mickael Ohanna^{1,2} , Ana Popovic^{1,2}, Aude Mallavialle^{1,2}, Frédéric Larbret^{1,2}, Sabrina Pisano³ , Stéphane Audebert⁴ , Thierry Passeron^{1,5}, Cédric Gaggioli³, Christophe A Girard^{1,2}, Marcel Deckert^{1,2,*†}  & Sophie Tartare-Deckert^{1,2,**†} 

Abstract

Resistance to BRAF/MEK inhibitor therapy in BRAF^{V600}-mutated advanced melanoma remains a major obstacle that limits patient benefit. Microenvironment components including the extracellular matrix (ECM) can support tumor cell adaptation and tolerance to targeted therapy; however, the underlying mechanisms remain poorly understood. Here, we investigated the process of matrix-mediated drug resistance (MMDR) in response to BRAF^{V600} pathway inhibition in melanoma. We demonstrate that physical and structural cues from fibroblast-derived ECM abrogate anti-proliferative responses to BRAF/MEK inhibition. MMDR is mediated by drug-induced linear clustering of phosphorylated DDR1 and DDR2, two tyrosine kinase collagen receptors. Depletion and pharmacological targeting of DDR1 and DDR2 overcome ECM-mediated resistance to BRAF-targeted therapy. In xenografts, targeting DDR with imatinib enhances BRAF inhibitor efficacy, counteracts drug-induced collagen remodeling, and delays tumor relapse. Mechanistically, DDR-dependent MMDR fosters a targetable pro-survival NIK/IKK α /NF- κ B2 pathway. These findings reveal a novel role for a collagen-rich matrix and DDR in tumor cell adaptation and resistance. They also provide important insights into environment-mediated drug resistance and a preclinical rationale for targeting DDR signaling in combination with targeted therapy in melanoma.

Keywords DDR; extracellular matrix; melanoma; NF- κ B2; therapeutic resistance

Subject Categories Cancer; Skin

DOI 10.15252/emmm.201911814 | Received 26 November 2019 | Revised 8 December 2021 | Accepted 9 December 2021 | Published online 27 December 2021

EMBO Mol Med (2022) 14: e11814

Introduction

One of the hallmarks of cancer cells is their remarkable ability to adapt to microenvironmental influences, such as the nature of the stroma including the extracellular matrix (ECM) and therapeutic stress (Pickup *et al*, 2014). This is particularly true for malignant cutaneous melanoma, which is one of the most aggressive and refractory human cancers (Shain & Bastian, 2016). Approximately 50% of melanoma carries activating mutations in the *BRAF* oncogene, leading to the activation of the mitogen-activated protein kinase (MAPK)/ERK pathway. Inhibition of the BRAF^{V600E/K} oncoprotein by BRAF inhibitors (BRAFi) such as vemurafenib or dabrafenib has markedly improved clinical outcome of patients (Flaherty *et al*, 2012). Despite this, durable responses are rare as most patients relapse within a year of beginning the treatment. Significant prolonged benefit can be achieved by combining BRAFi and MEK (MAPK/ERK kinase) inhibitors (MEKi) such as cobimetinib or trametinib, yet the development of drug resistance remains the most common clinical outcome (Robert *et al*, 2019). Acquired resistance to targeted therapies involves genetic alterations in key intracellular regulators of the MAPK signaling pathway. This leads to the restoration of the pathway and non-genetic alterations that are commonly

1 Université Côte d'Azur, INSERM, C3M, Nice, France

2 Equipe labellisée Ligue Contre le Cancer, Team MicroCan, Nice, France

3 Université Côte d'Azur, CNRS, INSERM, IRCAN, Nice, France

4 Aix-Marseille University, CNRS, INSERM, Institut Paoli-Calmettes, CRCM, Marseille, France

5 Université Côte d'Azur, Centre Hospitalier Universitaire de Nice, Department of Dermatology, Nice, France

*Corresponding author. Tel: +33 489153850; E-mail: deckert@unice.fr

**Corresponding author. Tel: +33 489153851; E-mail: tartare@unice.fr

†These authors contributed equally to this work as senior authors

associated with transcriptional reprogramming and phenotype switching from a melanocytic to an invasive undifferentiated mesenchymal-like cell state, which is characterized by lower expression levels of MITF and SOX10 and higher levels of AXL (Muller *et al*, 2014; Rambow *et al*, 2019). Such adaptive responses to BRAF oncogenic pathway inhibition are thought to precede mutation-driven acquired resistance (Smith *et al*, 2016).

However, in addition to mechanisms of resistance intrinsic to cancer cells, dynamic, *de novo* mechanisms exist, which are orchestrated by the tumor microenvironment and occur during the cancer cell's adaptation to therapy. Environment-mediated drug resistance (EMDR) thus appears as an important contributor to how cancer cells escape therapies (Meads *et al*, 2009). This process has initially been described in multiple myeloma and other hematopoietic malignancies and was shown related to minimal residual disease. This phenomenon is gaining importance in the field of melanoma with several studies reporting the involvement of stroma-derived factors in adaptive response and resistance to targeted therapies (Straussman *et al*, 2012; Fedorenko *et al*, 2015; Hirata *et al*, 2015; Kaur *et al*, 2016; Young *et al*, 2017). Given the key role of EMDR enabling the emergence of genetic resistance, an understanding and further identification of EMDR mechanisms in melanoma may assist with the development of more effective therapeutic strategies, thereby increasing the efficacy of targeted therapies.

Tumors are complex and adaptive ecosystems that are affected by numerous stromal components, which enhance tumor phenotypes and therapy resistance. Cancer-associated fibroblasts (CAFs) are activated fibroblasts and the primary producers of ECM. The ECM is a highly dynamic structural framework of macromolecules, providing both biochemical and biomechanical cues, which are required for tumor progression (Kalluri, 2016). The ECM is primarily composed of fibrillar and non-fibrillar collagens, hyaluronic acid, proteoglycans, and adhesive glycoproteins such as fibronectin, thrombospondins, and SPARC. It also contains matrix-remodeling enzymes and other ECM-associated proteins and acts as a reservoir for cytokines and growth factors (Hynes & Naba, 2012; Mouw *et al*, 2014). ECM composition, fiber orientation, and physical characteristics are profoundly altered in the vast majority of solid tumors (Pickup *et al*, 2014). Interactions between cells and the ECM elicit intracellular signaling pathways and regulate gene transcription, mainly through cell-surface adhesion receptors including integrins and discoidin domain receptors (DDR). DDR1 and DDR2 belong to a unique subfamily of receptor tyrosine kinases and have been identified as non-integrin collagen receptors (Shrivastava *et al*, 1997; Vogel *et al*, 1997; Leitinger, 2014). They are distinguished from each other by their relative affinity for different types of collagens, as DDR1 is activated by both fibrillar and non-fibrillar collagens, whereas DDR2 is only activated by fibrillar collagens. Furthermore, their expression and function are associated with fibrotic disease and cancer (Valiathan *et al*, 2012; Leitinger, 2014). DDR1 or DDR2 is known to control tumor cell proliferation and invasion, depending on the tumor type and the nature of the microenvironment (Valiathan *et al*, 2012). However, the functional role of DDR activity in mediating sensitivity to anti-cancer therapies and tumor resistance is poorly documented.

Adhesion of tumor cells to the ECM is a key component of EMDR. However, the influence of matrix-mediated drug resistance (MMDR) in response to targeted therapies and the nature of ECM

receptors driving the MMDR phenotype in melanoma have not yet been addressed in detail. To model the contribution of the ECM in melanoma cell responses to BRAF and MEK inhibition, we generated fibroblast-derived 3D ECM from melanoma-associated fibroblasts (MAFs), which were isolated from patient-derived biopsies and analyzed the MMDR mechanism with the aim to identify novel opportunities for microenvironment-targeted therapies. Here, we show that DDR1 and DDR2 are key mediators of MMDR in melanoma, through the pro-survival non-canonical NF- κ B2 pathway. Our findings reveal a novel role for these collagen-activated tyrosine kinase receptors, in mediating BRAF inhibitor tolerance. These data therefore support the rationale to inhibit DDR1 and DDR2 signaling, to disrupt the therapy-resisting properties conferred by the ECM in the microenvironment. We propose that the use of DDR inhibitors as a novel combinatorial therapeutic strategy may be beneficial for melanoma patients in overcoming resistance to MAPK-targeted therapy.

Results

Fibroblast-derived 3D ECM confers drug-protective action to melanoma cells against anti-BRAF^{V600E} therapies

To investigate the potential contribution of MMDR to targeted therapy in BRAF-mutated melanoma cells, we employed an *in vitro* model based on live cell-derived 3D ECMs. These matrices mimic many structural and biomolecular features, which are typically found *in vivo* (Cukierman *et al*, 2001). We selected human primary fibroblasts obtained from healthy individuals or MAFs isolated from patient metastatic melanoma biopsies (MAFs) in either the skin or lymph nodes (LN). The different fibroblast cultures were functionally tested in a 3D collagen matrix contraction assay, which showed that unlike human dermal fibroblasts (HDF), skin and LN MAF displayed actomyosin contractile activity. Similar to MAFs, LN normal fibroblasts known as fibroblastic reticular cells (FRC) are myofibroblast-like cells (Fletcher *et al*, 2015), which also showed a high propensity to contract collagen (Fig 1A). Cell-derived matrices were then generated and de-cellularized, and their composition, architecture, and rigidity were analyzed using proteomic and microscopic approaches. In our experimental conditions, compared to HDF, skin and LN MAF, as well as FRC, produced and assembled a dense 3D ECM composed of oriented collagen and fibronectin fibers, as shown by picrosirius red and immunofluorescence staining of the ECMs (Fig 1B). Proteomic analysis of the different fibroblast-derived ECMs further documented the molecular composition of these matrices, showing enrichment for several types of collagens and core matrix components including glycoproteins, proteoglycans, and ECM regulators and ECM-associated proteins (Appendix Fig S1). Atomic force microscopy (AFM) analysis of ECM stiffness revealed values for MAF and HDF matrices that were within the range of previous observations (Kaukonen *et al*, 2016; Fig 1C). We noticed that matrices generated from FRC and MAF were stiffer than HDF-derived ECM. Collectively, these observations validate the use of our experimentally derived matrices for functional studies. Next, we tested the effectiveness of the fibroblast-derived ECMs generated from HDF, FRC, or MAF to protect BRAF^{V600E}-mutated melanoma cells against the anti-proliferative effect of MAPK pathway

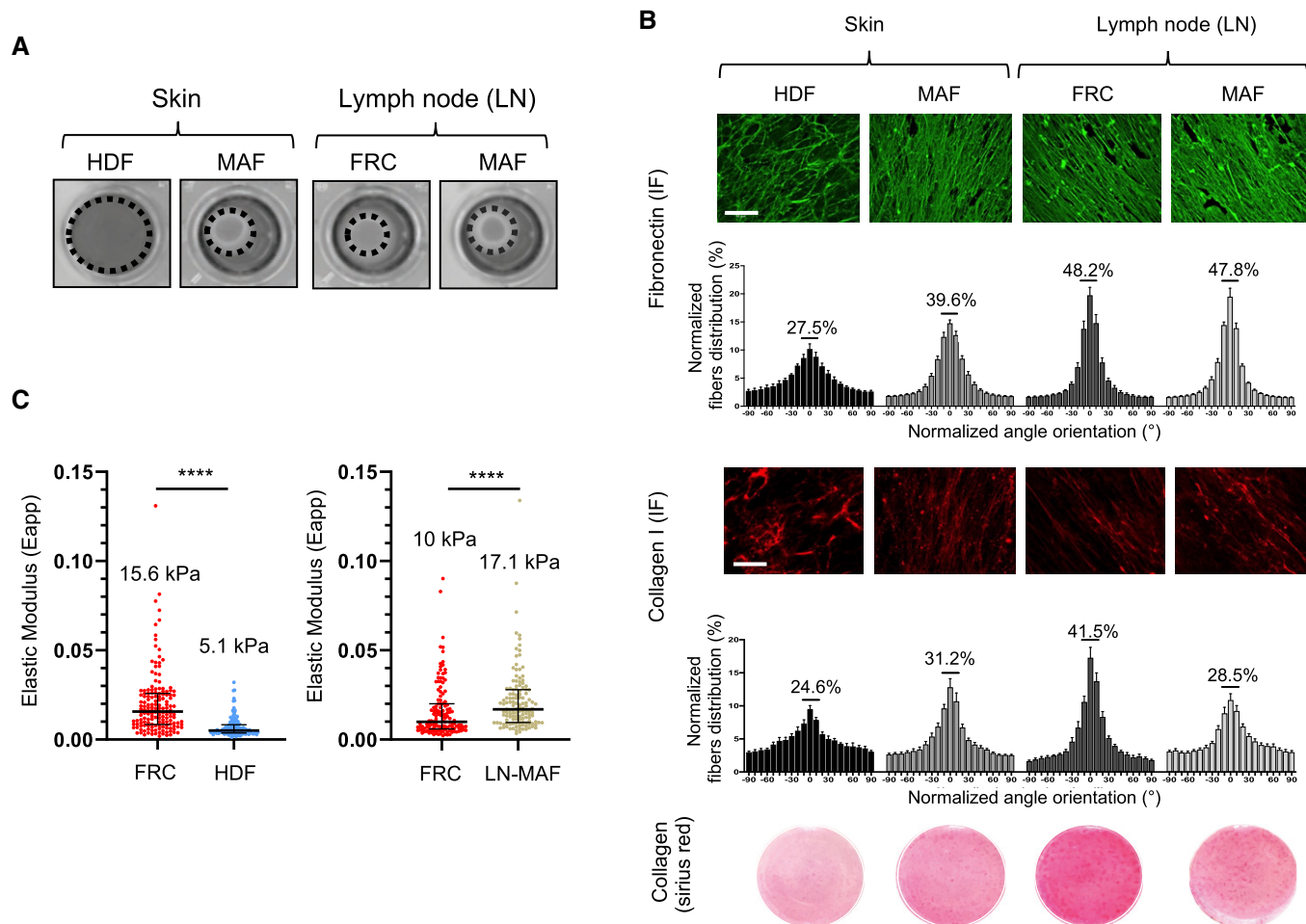


Figure 1. Composition, topology, and mechanical properties of fibroblast-derived 3D ECMs.

A Images show collagen matrix gel contraction by HDF (human dermal fibroblasts), skin-MAF (melanoma-associated fibroblasts isolated from skin lesions), LN-FRC (lymph node fibroblast reticular cells), and LN MAF (melanoma-associated fibroblasts isolated from metastatic lymph node). Dashed circles represent the diameter of the gel. Data are representative of $n = 3$ independent experiments.

B Immunofluorescence analysis of fibronectin (green) and collagen (red) fibers on de-cellularized ECM produced by human fibroblasts. Fiber orientation was quantified using ImageJ software. Percentages indicate oriented fibers accumulated in a range of $\pm 21^\circ$ around the modal angle. Data are represented as mean \pm s.d. ($n = 10$ random fields from 2 independent determinations). Scale bar, 50 μm . A representative image of picrosirius red staining from 10 analyzed images is shown for each condition.

C Atomic force microscopy (AFM) measurement of the elastic properties (apparent Young's modulus, E_{app}) of fibroblast-derived ECMs. Each dot represents a specific Young's modulus obtained by fitting the corresponding individual force curve acquired on a determined point of the sample. A representative experiment from 2 independent experiments is shown. Scatter plots show mean \pm SEM. The black bars represent the median and the interquartile range. **** $P < 0.0001$, two-tailed Mann-Whitney test.

inhibition. We therefore developed a drug-protective assay based on the culture of melanoma cells that stably expressed a fluorescent nuclear label, cultured on top of fibroblast-derived ECMs (Fig 2A). Tumor cells were then treated with drugs targeting the mutant BRAF/MAPK pathway using BRAFi alone or in combination with MEKi (Fig 2B). Cell proliferation was monitored using live cell time-lapse imaging and quantified by counting the number of fluorescent nuclei. Cell growth inhibition induced by BRAFi alone (vemurafenib) or in combination with MEKi (trametinib) was abrogated when 1205Lu melanoma cells were cultured on top of fibroblast-derived ECMs, in sharp contrast to standard cell culture conditions where cells were plated either on plastic or on purified collagen 1

(Coll-1) (Figs 2C and D, and EV1A). In line with the organization of the 3D matrices depicted in Fig 1, drug-protective assays against BRAFi or BRAFi/MEKi combo-therapy revealed that MAF- and FRC-derived matrices display higher protective abilities compared to HDF-derived ECMs and conferred increased protection (Figs 2D and EV1A). Similar protective effects were observed with the SKMEL5 cell line and the MM099 patient-derived short-term melanoma culture when these cells were plated on the different experimental ECM settings (Figs 2E and EV1B). These data suggest that MMDR relies on the topological and molecular features of the ECM. Cell cycle analysis in SKMEL5 and MM099 cells further showed that experimentally produced ECM from HDF, MAF, or FRC prevented

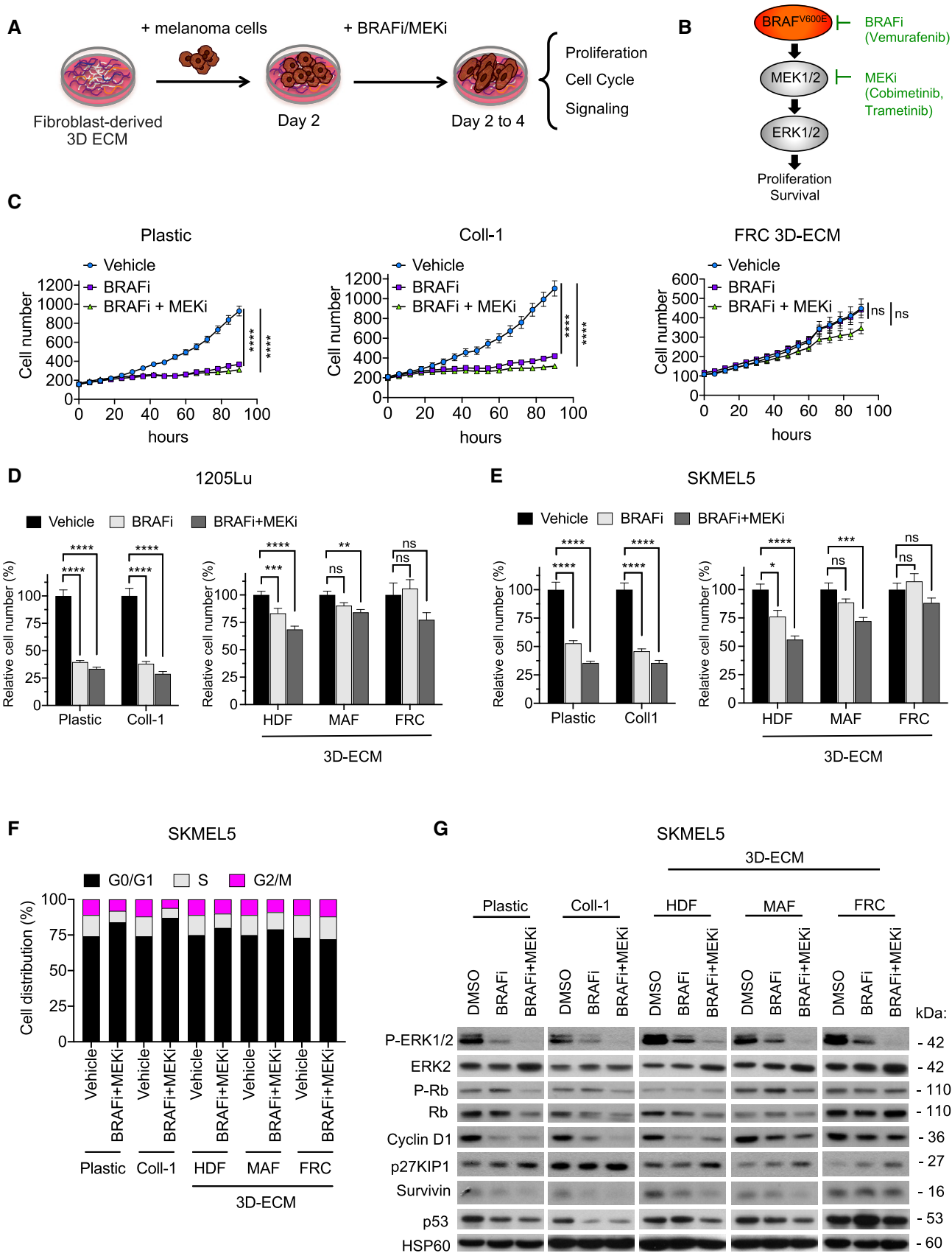


Figure 2.

Figure 2. Fibroblast-derived 3D ECM confers drug-protective action to melanoma cells against anti-BRAF^{V600} therapies.

- A Scheme of the ECM-mediated drug-protective assay.
- B Illustration of the BRAF^{V600E} pathway and the MAPK pathway inhibitors used in the study.
- C Time-lapse imaging of proliferation of NuLight-labeled 1205Lu cells plated on plastic (left panel), Coll-1 (collagen 1; middle panel), or FRC-derived ECM (right panel) and treated with vehicle, 5 μ M BRAFi, or 2 μ M BRAFi plus 0.01 μ M MEKi using the IncuCyte ZOOM system. Each data point represents the mean of NuLight red nuclear objects per field \pm SEM. **** P < 0.0001, two-way ANOVA followed by Dunnett's multiple comparisons test. Data are representative of $n = 3$ independent experiments.
- D, E Quantification of proliferation of 1205Lu (D) and SKMEL5 (E) cells plated for 48 h on plastic, Coll-1, or the indicated fibroblast-derived ECMs prior to a 96-h treatment with vehicle, 5 μ M BRAFi, or 2 μ M BRAFi plus 0.01 μ M MEKi. Cells were counted by Hoechst-labeled nuclei staining. Data are represented as bar plots with mean \pm SEM normalized to vehicle of 3 independent experiments. (D) ** P = 0.015, *** P = 0.0009, and **** P < 0.0001; and (E) * P = 0.0204, *** P = 0.0006, and **** P < 0.0001, the Kruskal–Wallis test followed by Dunn's multiple comparisons test.
- F Flow cytometry analysis of cell cycle distribution of SKMEL5 cells cultured on plastic, Coll-1, or the indicated fibroblast-derived ECMs and treated with vehicle or 2 μ M BRAFi combined with 0.01 μ M MEKi. The percentage of cells in different phases of the cell cycle is indicated.
- G Immunoblotting of protein extracts from SKMEL5 cells cultivated as described above on plastic, Coll-1, or the indicated fibroblast-derived ECMs in the presence or not of BRAFi or BRAFi/MEKi for 96 h, using antibodies against p-ERK1/2, ERK2, or cell cycle markers (p-Rb, Rb, cyclin D1, p27KIP1, survivin, and p53). HSP60, loading control.

Source data are available online for this figure.

the G0/G1 cell cycle arrest, induced by the BRAFi/MEKi cocktail in contrast to the cell culture conditions on plastic or Coll-1-plated dishes (Figs 2F and EV1C). The ECM therefore transmits signals that prevent the cytostatic action of MAPK pathway inhibitors. At the molecular level, ECM-mediated therapeutic escape of SKMEL5, 1205Lu, and MM099 cells from BRAF pathway inhibition was associated with sustained levels of the proliferation markers phosphorylated Rb, cyclin D1, and survivin, and lower levels of the cell cycle inhibitor p27KIP1, although ERK1/2 phosphorylation was similarly decreased in the presence of the targeted drugs in all culture conditions (Figs 2G and EV1D). Immunoblot analysis also suggested that upon BRAF inhibition, the levels of proliferative markers were higher in melanoma cells on MAF- and FRC-derived ECMs than on HDF-derived ECMs. In contrast, no significant changes in p53 levels were observed. Together, these results indicate that fibroblasts assembled and remodeled matrices that provide a drug-tolerant environment for BRAF mutant melanoma cell lines and short-term cultures.

Expression of the collagen receptors DDR1 and DDR2 in melanoma

Previous studies have demonstrated the critical role of ECM receptors belonging to the integrin family in drug resistance (Seguin *et al*, 2015). Moreover, BRAF inhibition has been described to generate a drug-protective stroma with high β 1 integrin/FAK signaling, as a

result of the paradoxical action of BRAFi on MAF (Hirata *et al*, 2015). Yet, in our experimental conditions, we were unable to show a significant implication of the β 1 integrin/FAK axis in drug protection conferred by fibroblast-derived ECMs. Indeed, the addition of blocking β 1 integrin antibodies and the depletion of FAK both failed to prevent the protective properties of fibroblast-derived ECM against the growth and survival inhibitory signals induced by BRAFi (Appendix Fig S2).

This finding prompted us to interrogate the contribution of other ECM receptors in targeted therapy resistance. Keeping in mind the elevated levels of fibrillar collagens found in fibroblast-derived ECMs (Fig 1B; Appendix Fig S1), we examined the functional implication of the collagen tyrosine kinase receptors DDR1 and DDR2 (Shrivastava *et al*, 1997; Vogel *et al*, 1997). The analysis of TCGA datasets for cutaneous melanoma showed that the *DDR1* and *DDR2* genes were genetically altered in 20% and 13% of melanoma cases, respectively. Interestingly, a significant fraction of melanomas was found to be associated with an amplification of DNA copy number and higher mRNA levels of *DDR1* and *DDR2* (respectively 13% and 10% of samples) (Fig 3A). This is consistent with the notion that these collagen receptors may play an important role in melanoma pathogenesis. Immunohistochemical analysis of *DDR1* and *DDR2* expression in benign nevi and malignant primary and metastatic melanocytic skin lesions further showed that *DDR1* and *DDR2* levels significantly increased during melanoma progression, indicating that *DDR1* and *DDR2* may represent novel prognostic factors for

Figure 3. Expression of DDR1 and DDR2 in human melanoma.

- A Meta-analysis of 363 cutaneous melanoma from TCGA (skin cutaneous melanoma, PanCancer Atlas) (<http://www.cbioportal.org/>) showing the percentage of samples with genetic alterations in *DDR1* and *DDR2*. Cases with missense (green) and truncating (blue) mutations, amplification (red), and mRNA overexpression (pink) are indicated; gray, individual cases.
- B Immunohistochemical analysis of *DDR1* and *DDR2* levels on human melanoma tissue microarrays. Representative IHC images and quantification (right bar histograms) of *DDR1* and *DDR2* expression in normal skin, nevus, primary melanoma (PM), and lymph node melanoma metastases (MM). Scale bar, 100 μ m. Histological scoring of the samples was performed in a blinded fashion. Samples were scored as low, medium, or high for *DDR1* or *DDR2* expression (nevus, $n = 12$; PM, $n = 30$; and MM, $n = 20$).
- C–E Immunoblotting of equal amounts of protein extracts from melanoma cell lines (C), patient-derived short-term cell cultures (D), or isogenic pairs of parental-sensitive and BRAFi-resistant cell lines (E) using antibodies against *DDR1*, *DDR2*, or markers of the melanoma cell differentiation *AXL*, *MITF*, or *SOX10*. ERK2, loading control.
- F *DDR1* and *DDR2* levels increase in de-differentiated melanoma cells. Box-and-whisker plots show *DDR1*, *DDR2*, *MITF*, *AXL*, and *SOX10* expression among four differentiation melanoma cell states (U, undifferentiated, $n = 10$; NC, neural crest-like, $n = 14$; T, transitory, $n = 12$; and M, melanocytic, $n = 17$) (GSE80829). The expression of *AXL*, *MITF*, and *SOX10* is shown as control markers of cell differentiation. n , number of cell lines representative of each cell state. Central bars represent the median, and the whiskers, the 10th to 90th percentile of the boxplot. Multiple comparisons were performed using ordinary one-way ANOVA.

Source data are available online for this figure.

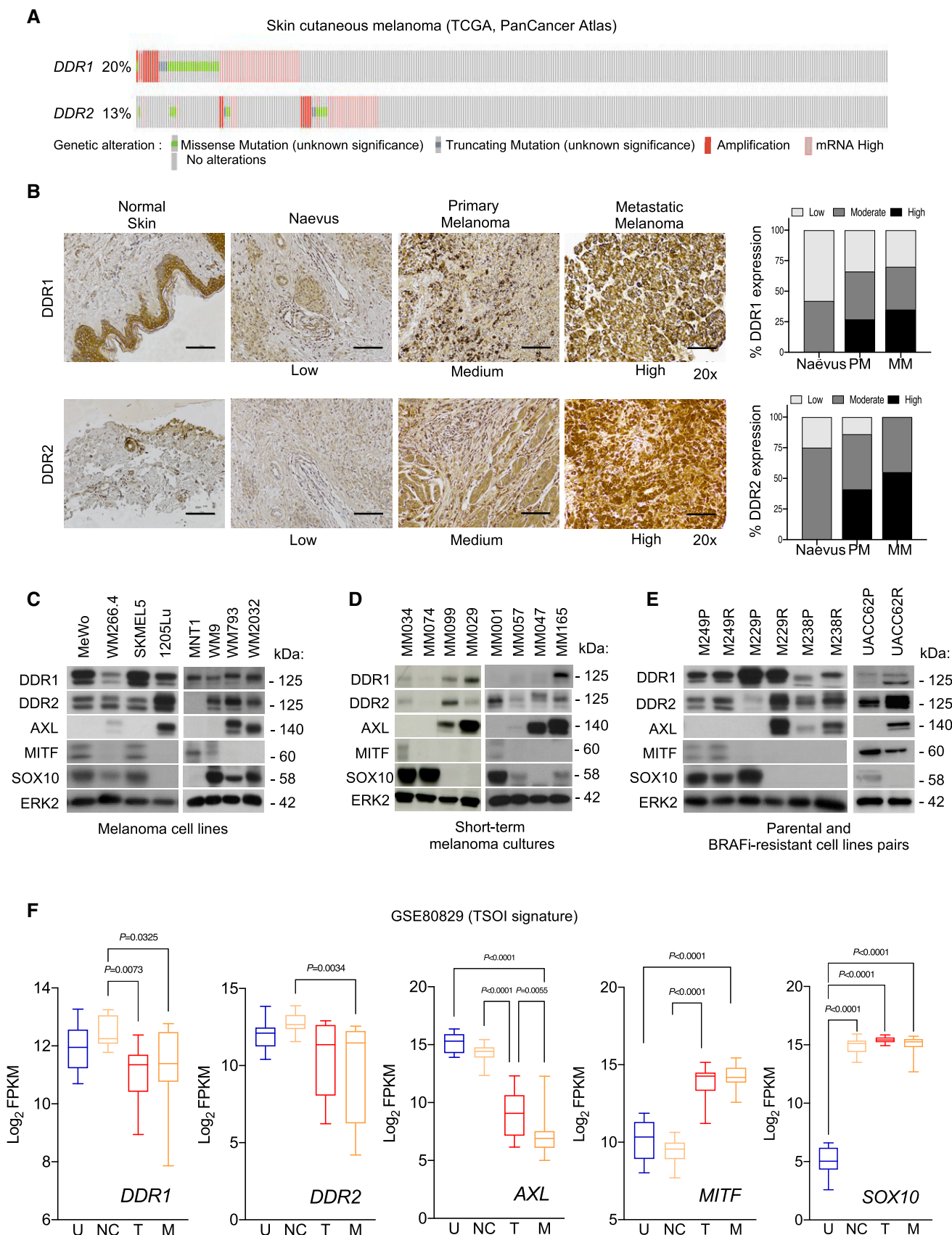


Figure 3.

melanoma (Fig 3B; Appendix Fig S3). We next examined the levels of DDR1 and DDR2 in a collection of melanoma cell lines and short-term melanoma cultures in relation to the cell state differentiation markers MITF, SOX10, and AXL. DDR1 and DDR2 were both expressed in melanoma cell lines regardless of their differentiation of cell phenotype (Fig 3C). In patient-derived short-term melanoma cultures, higher DDR1 and DDR2 protein levels were detected in BRAF mutant MM099 and MM029 and NRAS mutant MM165 cells with the MITF^{low}, SOX10^{low}, and AXL^{high} de-differentiated phenotype signature (Fig 3D). Moreover, higher levels of DDR2 were found to be associated with lower levels of the melanocytic marker MITF and higher levels of the drug-resistant marker AXL in de-differentiated mesenchymal-like BRAFi-resistant M229R, M238R, and UACC62R cells compared to their parental counterparts (Nazarian *et al*, 2010; Girard *et al*, 2020; Misek *et al*, 2020) (Fig 3E). The examination of public gene expression datasets of the melanoma differentiation signature confirmed that *DDR1* and *DDR2* levels were increased in the undifferentiated (U) and neural crest-like (NC) cell subpopulations from the TSOI signature (Fig 3F; Tsoi *et al*, 2018) and in the invasive MITF^{low} cells from the HOEK signature (Appendix Fig S4; Widmer *et al*, 2012). De-differentiated/undifferentiated melanoma cells display intrinsic resistance to MAPK pathway inhibition (Muller *et al*, 2014; Tsoi *et al*, 2018; Rambow *et al*, 2019). In line with this notion, we found that DNA amplification and elevated mRNA levels of *DDR1* negatively correlated to the activity of BRAF and MEK inhibitors in melanoma cell lines from the GDSC (Genomic of Drug Sensitivity in Cancer) (Appendix Fig S5). Together, these observations associate DDR expression with melanoma progression and with the invasive and therapy-resistant phenotype.

Targeting DDR impairs ECM-mediated resistance to oncogenic BRAF pathway inhibition

Next, we compared how fibroblast-derived ECMs modulate DDR phosphorylation, an event linked to their activity (Shrivastava *et al*, 1997; Vogel *et al*, 1997). Immunoblot analysis of lysates from 1205Lu and MM099 cells plated on MAF- and FRC-derived ECMs indicated that MAF-derived matrices have a stronger ability to increase the levels and phosphorylation of DDR1 and/or DDR2

compared to HDF-derived matrices (Fig EV2A), supporting a functional implication of DDR in melanoma drug tolerance. Interestingly, while BRAF and/or MEK inhibition had no significant effect on DDR phosphorylation in 1205Lu cells cultivated on MAF-derived ECM, MEK inhibition seemed to increase DDR1 expression levels (Appendix Fig S6). To address the contribution of DDR in MMDR, a siRNA approach was then used to target DDR1, DDR2, or both in melanoma cells cultured on MAF- or FRC-derived ECMs, in the presence of BRAFi alone or in combination with MEKi. Immunoblot analysis showed specific DDR1 and DDR2 protein reduction after siRNA transfection using two different targeted sequences in BRAFi-treated 1205Lu cells cultured on MAF- or FRC-derived ECMs (Figs 4A and EV2B). Compared to the single knockdown, the simultaneous knockdown of DDR1 and DDR2 overcame MMDR to BRAF-targeted therapy as revealed by decreased levels of cell proliferation markers, including phosphorylated Rb, survivin, and E2F1, in 1205Lu and SKMEL5 cells (Fig 4A and B). Importantly, depletion of both DDR1 and DDR2 enhanced the cytotoxic activity of co-targeting BRAF/MEK as shown by the increased cleavage of apoptotic caspase-3 that was detected in SKMEL5 and MM099 melanoma cells (Figs 4B and EV2C). DDR are druggable receptors targeted by imatinib, a tyrosine kinase inhibitor (TKI) initially developed as an ABL inhibitor, which also inhibits DDR activity with high efficacy (Day *et al*, 2008). Imatinib belongs to therapeutic molecules used in the clinic for the treatment of chronic myeloid leukemia and acute lymphoblastic leukemia with the Philadelphia chromosome (Druker *et al*, 2001). Enzymatic activities of DDR were also inhibited by other small molecules including DDR1-IN-1 (Kim *et al*, 2013). We first confirmed that imatinib and DDR1-IN-1 efficiently inhibited type I collagen-induced DDR1 and DDR2 tyrosine phosphorylation in 1205Lu cells (Fig EV2D). Inhibition of DDR1/2 kinases by imatinib or DDR1-IN-1 suppressed the protective action of MAF- and FRC-derived ECMs against BRAF inhibition, as evidenced by the significant decrease in 1205Lu cell proliferation, which was observed after co-treatment with BRAFi and DDR1/2 inhibitors (Figs 4C and EV2E). Similar anti-proliferative effects of DDR inhibitors were observed during drug-protective assays performed in SKMEL5 and MM099 cells on MAF- or FRC-derived ECMs (Fig EV2F and G). Mutant BRAF and DDR1/2 co-targeting in the three melanoma cell lines plated on FRC- or MAF-derived ECMs decreased levels of phosphorylated Rb, E2F1, and survivin, and induced

Figure 4. Inhibition of DDR1 and DDR2 by genetic or pharmacological approaches abrogates ECM-mediated resistance to BRAF^{V600} pathway inhibition.

- Immunoblotting of protein extracts from 1205Lu cells transfected with a siRNA control (CTRL) or two different sequences of siRNA (#1 and #2) directed against DDR1 or DDR2 alone or in combination prior to being cultivated on MAF-derived ECM and treated or not with 5 μ M BRAFi for 96 h, using antibodies against the indicated proteins. HSP60, loading control.
- Immunoblotting of protein extracts from SKMEL5 cells transfected with siCTRL or the combination of siDDR1#2 and siDDR2#2 prior to being cultivated on FRC- or MAF-derived ECMs (left and right panels, respectively) and treated with vehicle, 5 μ M BRAFi, or 2 μ M BRAFi plus 0.01 μ M MEKi, using antibodies against the indicated proteins. HSP60, loading control.
- Quantification of the time-lapse imaging of the proliferation of NucLight-labeled 1205Lu cells using the IncuCyte ZOOM system. Cells were plated for 48 h on FRC- or MAF-derived ECMs prior to a 96-h treatment with vehicle or 5 μ M BRAFi in the presence or not of 7 μ M imatinib or 1 μ M DDR1-IN-1. The bar plots represent the mean normalized to vehicle of NucLight red nuclear objects per field \pm SEM from 3 independent experiments performed in triplicate. **** P < 0.0001, two-way ANOVA followed by Sidak's multiple comparisons test.
- Immunoblotting of protein extracts from 1205Lu, SKMEL5, and MM099 cells plated for 48 h on FRC-derived ECM prior to a 96-h treatment with vehicle or 5 μ M BRAFi in the presence or not of imatinib (7 μ M for 1205Lu, 10 μ M for SKMEL5 and MM099) or DDR1-IN-1 (1 μ M for 1205Lu, 5 μ M for SKMEL5, and 3 μ M for MM099), using antibodies against the indicated proteins. HSP60, loading control.
- Flow cytometry analysis of cell death (Annexin V/PI labeling) in 1205Lu cells plated on FRC-derived ECM and treated as above. Right bar plots show the distribution of cells (% of total) across the different forms of death.

Source data are available online for this figure.

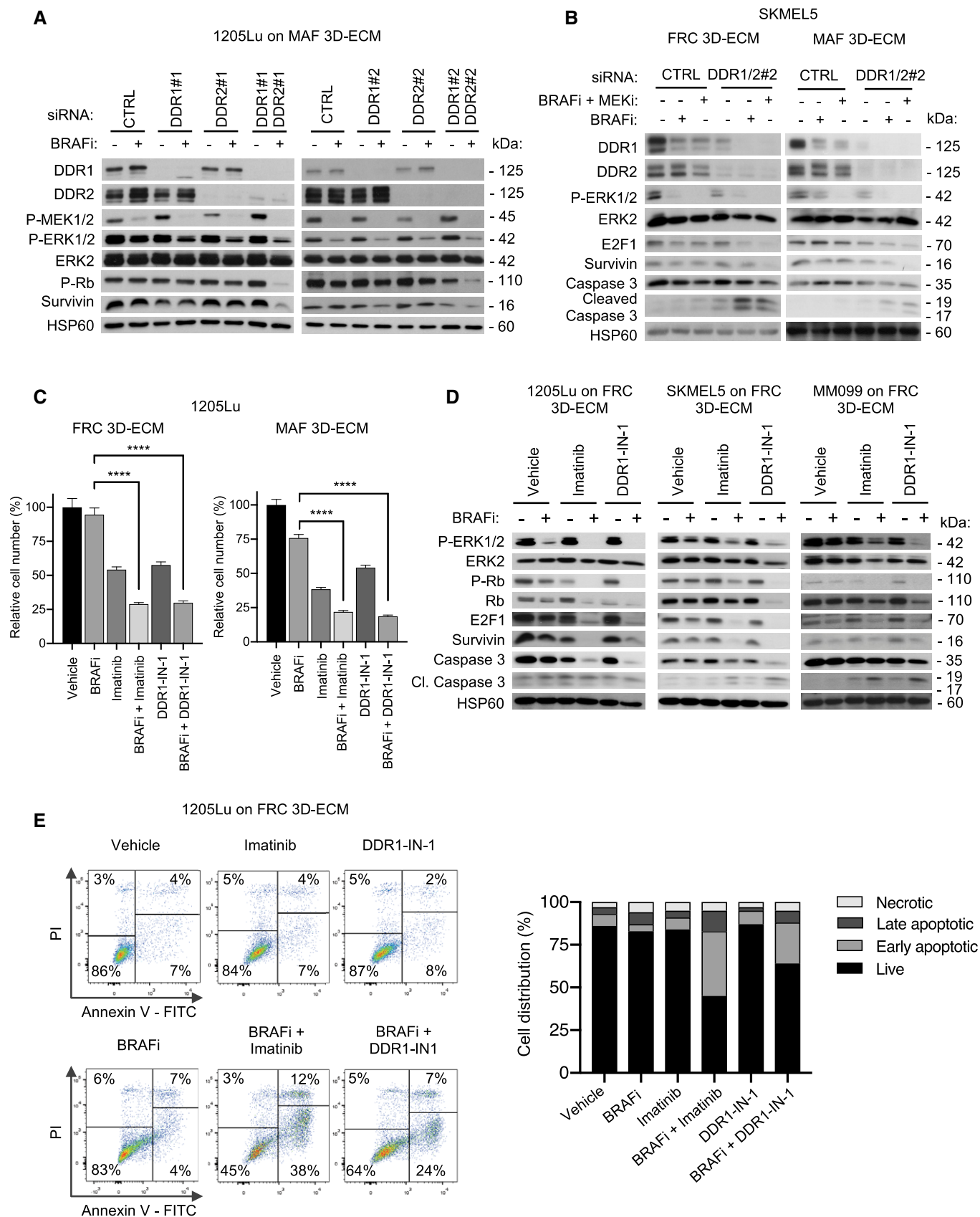


Figure 4.

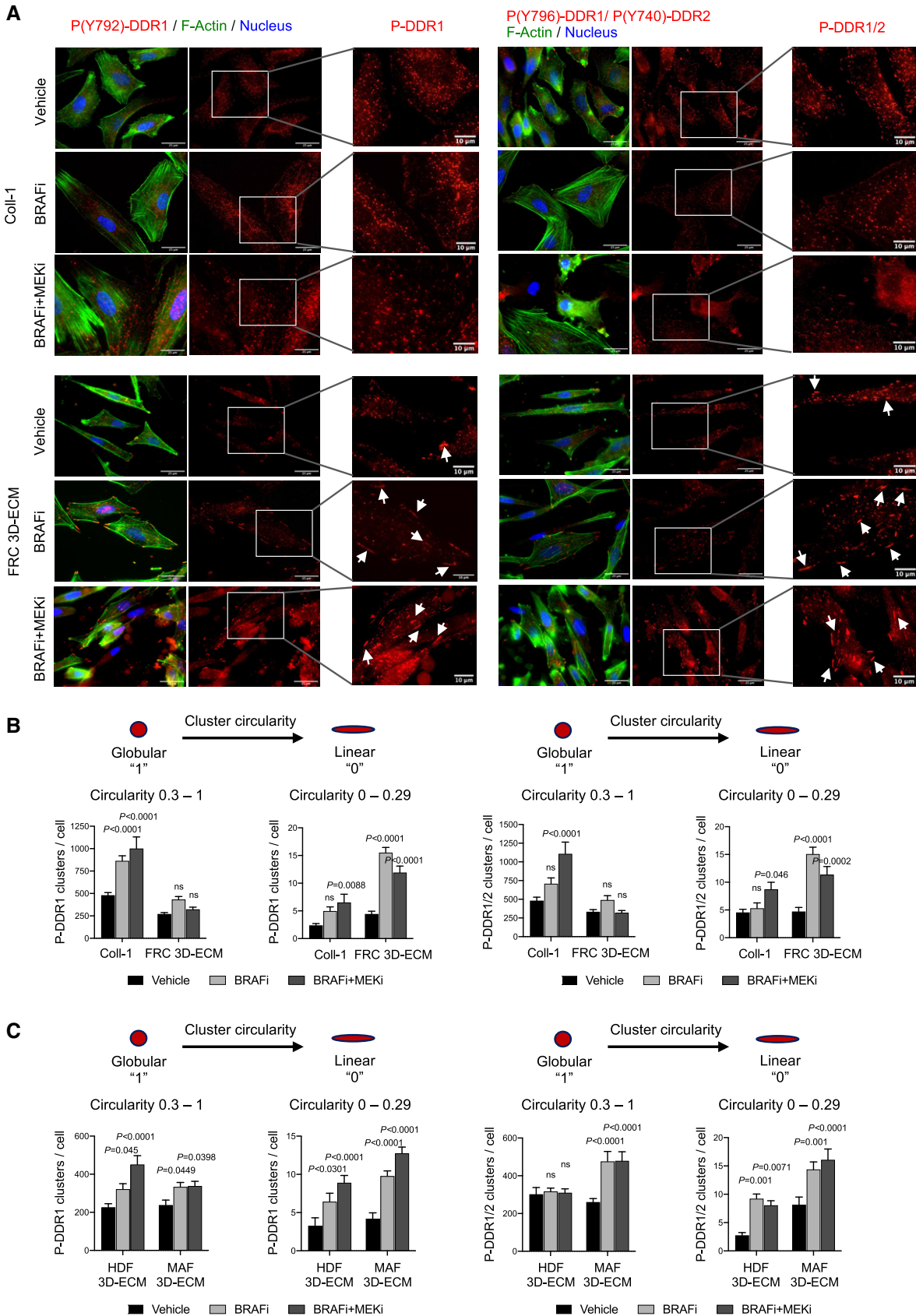


Figure 5.

Figure 5. Interaction of melanoma cells with 3D ECMs induces the linear clustering of phosphorylated DDR upon BRAFi/MEKi treatment.

- A Representative images of 1,205 cells cultivated on collagen I (Coll-I) or FRC-derived ECM for 48 h prior to treatment with vehicle or 5 μ M BRAFi or 2 μ M BRAFi plus 0.01 μ M MEKi for 96 h. Immunofluorescence for phospho-DDR1 (P(Y792)-DDR1) (red; left panels) and phospho-DDR1/2 (P(Y796)-DDR1/P(Y740)-DDR2) (red; right panels), F-actin (green), and nuclei (blue) is shown. Enlarged images of P-DDR1 and P-DDR1/2 immunostaining are shown. White arrows indicate P-DDR1 and P-DDR1/2 cell membrane linear clustering. Scale bar, 25 μ m (enlarged images: scale bar, 10 μ m).
- B Quantification of globular versus linear clusters of phospho-DDR1 (left panels) and phospho-DDR1/2 (right panels) from immunofluorescence staining shown in (A) using ImageJ software. Prior to the quantification of DDR clusters, a “subtract background” function of ImageJ has been applied to all images. In order to quantify clusters, the IsoData threshold has been used. Clusters with circularity 0.3–1 have been defined as “globular”, and clusters with circularity 0–0.29 have been defined as “linear”. Data are from > 20 individual cells ($n = 3$). Error bars reflect mean \pm s.d. Values for each treated condition are compared to the vehicle control. 2-way ANOVA followed by Dunnett’s multiple comparisons test.
- C Quantification of globular versus linear clusters of Phospho-DDR1 and Phospho-DDR1/2 from immunofluorescence staining shown in Fig EV4A of 1205Lu cells cultivated on HDF- or MAF-derived ECM and treated with the indicated targeted drugs as described in (A). Data are from > 20 individual cells. Error bars reflect mean \pm s.d. Values for each treated condition are compared to the vehicle control. 2-way ANOVA followed by Dunnett’s multiple comparisons test.

Source data are available online for this figure.

caspase-3 cleavage (Figs 4D and EV3A and B). Similar biochemical events were promoted by BRAFi or with the combined BRAFi and MEKi treatment, in the presence of nilotinib, a next-generation BCR-ABL inhibitor that is approved for the treatment of imatinib-resistant patients and targeting DDR1/2 (Day *et al.*, 2008; Fig EV3C). Induction of apoptosis in co-treated melanoma cells was further confirmed using flow cytometry analysis of cell death markers (Figs 4E and EV3D).

Recent studies described that collagen binding to DDR leads to their activation and clustering into filamentous membrane structures that are associated with collagen fibrils (Yeung *et al.*, 2019). We thus examined the clustering and spatial distribution of phosphorylated DDR in melanoma cells plated on collagen I-coated plastic dishes or on 3D ECMs, in response to oncogenic BRAF pathway inhibition. To detect DDR1 and/or DDR2, we used an antibody that specifically recognizes phosphorylated DDR1 at Y792 and an antibody that not only recognizes phosphorylated DDR2 at Y740 but also cross-reacts with the phosphorylated DDR1 (Yeung *et al.*, 2019). Immunofluorescence staining of P-DDR1 and P-DDR1/2 revealed that 1205Lu cells, which were cultured on purified collagen I, displayed a globular dot-like distribution of these two receptors, whereas cells seeded on FRC-derived 3D ECMs exhibited a fraction of P-DDR distributed into linear membrane clusters (Fig 5A and B). Importantly, cell exposure to BRAFi or to BRAFi/MEKi combination therapy dramatically increased the proportion of P-DDR1 and P-DDR1/2 containing linear clusters, on FRC-derived 3D ECM, as well as F-actin remodeling (Fig 5A and B).

Notably, the formation of linear clusters of P-DDR1 and P-DDR1/2 upon MAPK pathway inhibition is also significantly increased in

cells plated on MAF-derived 3D ECMs compared to cells cultured on HDF-derived ECMs (Figs 5C and EV4A), and these clusters colocalized with collagen fibers (Fig EV4B). Similar observations on phosphorylated DDR clustering were obtained with SKMEL5 melanoma cells (Fig EV4C and D). These data suggest that therapy-induced cytoskeletal changes drive a linear clustering of phosphorylated DDR along collagen fibers and subsequently cause MMDR. These findings therefore suggest that DDR1 and DDR2 determine BRAF mutant melanoma cell responsiveness to BRAF-targeted therapy, with regard to ECM features and that the drug-tolerant action of DDR is dependent on their enzymatic activities and correlates with the formation of filamentous membrane structures.

Pharmacological inhibition of DDR by imatinib improves targeted therapy efficacy, counteracts drug-induced collagen remodeling, and delays tumor relapse

The anti-tumor activity of imatinib combined with the BRAFi vemurafenib was assessed in a preclinical xenograft melanoma model. BRAF-mutated melanoma cells (1205Lu) were subcutaneously xenografted into nude mice (CDX model), which were exposed to BRAFi, imatinib, or BRAFi plus imatinib (Fig 6A). As expected, BRAF inhibition induced a rapid tumor reduction, whereas imatinib alone did not display a significant anti-melanoma effect (Fig 6B). However, following 12 days, tumors treated with BRAFi alone had resumed growth, whereas the combination treatment with imatinib markedly delayed tumor relapse and led to a significant reduction in tumor volume (Fig 6B–D) and weight (Fig 6C). Immunohistochemical

Figure 6. Targeting DDR by imatinib sensitizes melanoma tumors to BRAF^{V600E} inhibition.

- A Outline of the experimental setup and treatment regimens.
- B 1205Lu cells were s.c.-inoculated into nude mice, and when tumors reached 75 mm³, mice were treated with the indicated mono- or combo-therapy for 30 days. Graphs show tumor growth following treatment by indicated drugs. Data shown are mean \pm SEM of tumor volume. Vehicle and imatinib groups, $n = 10$ tumors from 5 mice; vemu and vemu/imatinib groups, $n = 20$ tumors from 10 mice). **** $P < 0.0001$, two-way ANOVA followed by Tukey’s multiple comparisons test.
- C Scatter plot graphs showing the tumor weight upon treatment by the indicated mono- or combo-therapy. Error bars show mean \pm SEM of tumor weight ($n = 10$ –11 tumors from 6 mice per condition). *** $P = 0.0002$, the Kruskal–Wallis test followed by Dunn’s multiple comparisons test; ns, non-significant.
- D Immunofluorescence staining using anti-cleaved caspase-3 (red), anti-Ki67 (green), and DAPI in tumor sections of 1205Lu-derived xenografts from (B). Scale bar, 100 μ m. A microphotograph of the tumor size in each treated group is shown (representative of $n = 5$ –10 mice).
- E Kaplan–Meier survival curves of mice treated with vehicle, imatinib, BRAFi, or BRAFi plus imatinib. Median time to progression was 18, 20, 36, and 48 days, respectively. Log rank (Mantel–Cox) for BRAFi vs BRAFi/imatinib mesylate. **** $P < 0.0001$ and hazard ratio (log rank): 0.2403 (95% CI of ratio, 0.08123–0.7106).
- F Mouse body weight was measured at the indicated day. Data shown are mean \pm SEM ($n = 5$ –10 mice).

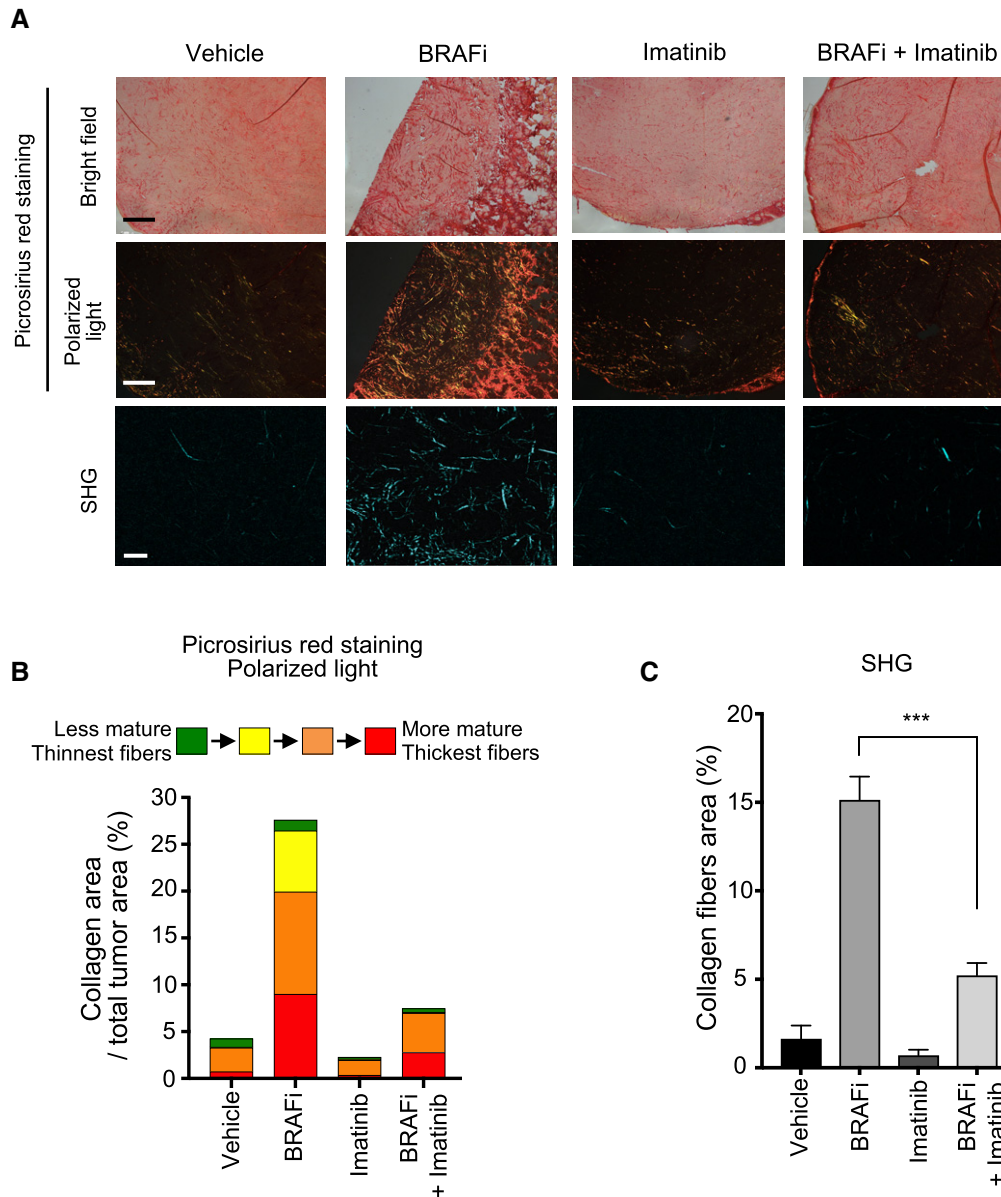


Figure 7. Imatinib normalizes collagen deposition and remodeling induced upon BRAFi treatment.

- A Sections of 1205Lu xenografts from Fig 6B were stained with picrosirius red and imaged under transmission light (upper panels) or polarized light (middle panels) (scale bar, 500 μ m) or imaged by second harmonic generation (SHG) microscopy (lower panels) (scale bar, 50 μ m) to examine collagen fiber network upon the mono- or combined regimens.
- B Quantification of collagen maturity and fiber thickness in 1205Lu xenografts stained with picrosirius red using polarized light microscopy. Birefringence hue and amount of collagen fibers were quantified as a percent of total tissue area (2–4 fields per tumor section, $n = 4$ tumors per condition).
- C Quantification of collagen fibers using SHG microscopy in tumor sections from (A). Error bars represent mean \pm s.d. of 4 independent fields per section, $n = 2$ tumors per condition. *** $P = 0.0002$, the Mann–Whitney test.

treatment with BRAFi (Jenkins *et al*, 2015; Girard *et al*, 2020), we next investigated collagen content and fiber organization in tumor tissues from mice treated with the different regimens. Histochemical analysis showed that BRAFi treatment triggered a profound remodeling of the melanoma stromal ECM (Fig 7A), with marked increase in the collagen fibers' area and thickness, which was suppressed by imatinib. Collagen color analysis under polarized light showed a decrease in mature orange and red fibers in tumors treated with the

combined regimen, compared to the single-agent treatment (Fig 7B). Finally, tumor imaging with second harmonic generation (SHG) confirmed the fibrillar nature of the collagen network that was rearranged upon BRAFi treatment but not upon the combined BRAFi and imatinib treatment (Fig 7A–C). These data suggest that treatment with imatinib counteracts the adverse effect of the targeted therapy on aberrant collagen deposition and organization, a process potentially contributing to drug resistance and relapse.

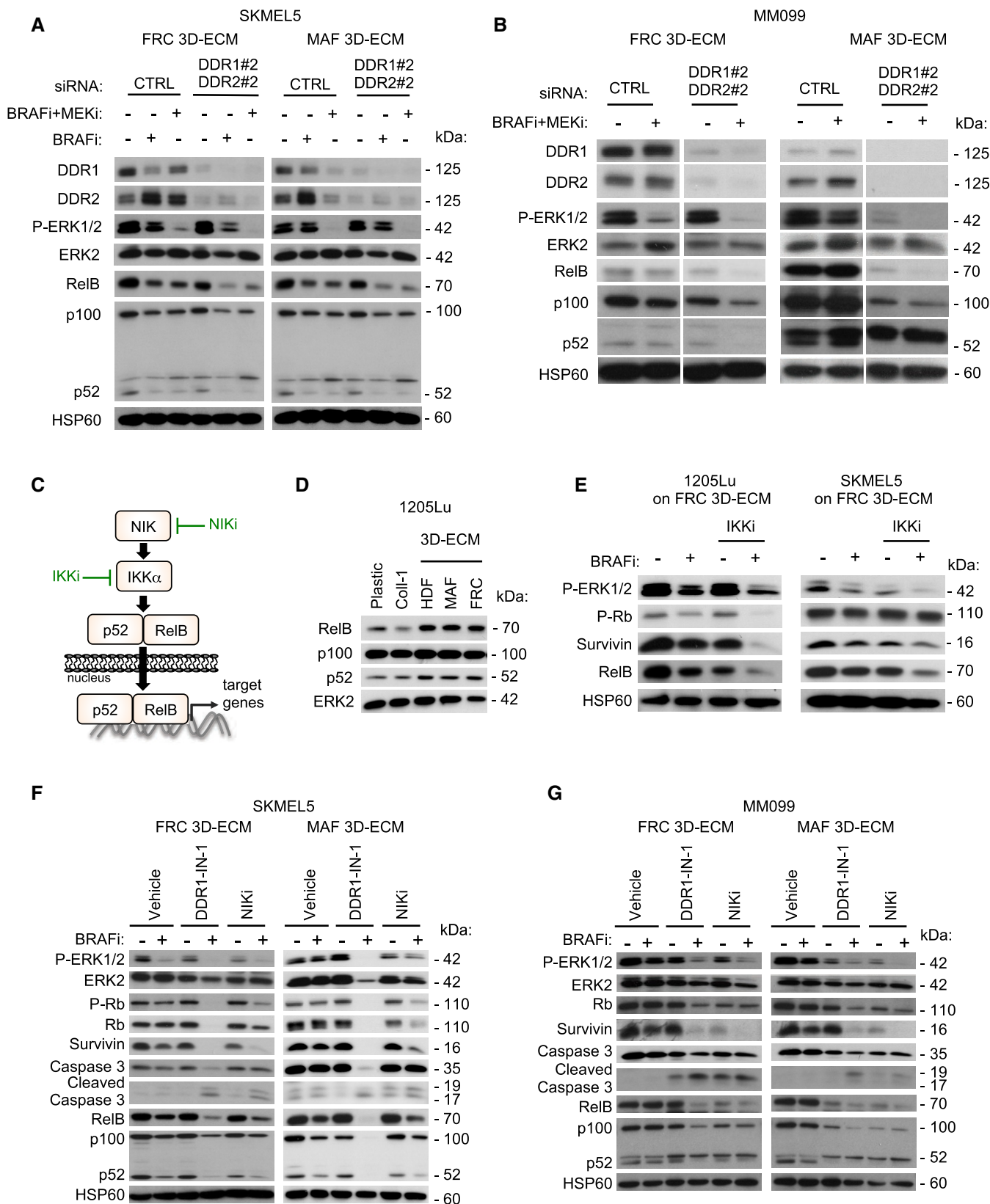


Figure 8.

Figure 8. Targeting the non-canonical NF- κ B2 pathway overcomes DDR-dependent MMDR to BRAF^{V600E} pathway inhibition.

- A Immunoblot analysis of protein extracts from siCTRL- or siDDR1/2-transfected SKMEL5 cells plated on FRC- or MAF-derived ECMs in the presence or not of 5 μ M BRAFi, 2 μ M BRAFi, plus 0.01 μ M MEKi for 96 h using antibodies against DDR1, DDR2, P-ERK1/2, ERK2, RelB, p100/p52, and HSP60 as loading control.
- B Immunoblot analysis of protein extracts from siCTRL- or siDDR1/2-transfected MM099 short-term cultures plated on FRC- or MAF-derived ECMs in the presence or not of 2 μ M BRAFi plus 0.01 μ M MEKi for 96 h using antibodies as above. Note that data come from the same immunoblot.
- C Illustration of the non-canonical p52/RelB NF- κ B2 pathway and inhibitors used in the study.
- D Immunoblot analysis of protein extracts from 1205Lu cells cultivated on plastic, Coll-1, or indicated fibroblast-derived ECMs for 48 h using antibodies against RelB, p100/p52, and ERK2 as loading control.
- E Immunoblot analysis of protein extracts from 1205Lu (left panels) or SKMEL5 (right panels) cells cultivated on FRC-derived ECMs for 96 h in the presence of 5 μ M BRAFi and/or a pan- IKK inhibitor (IKKi, BMS-345541 3 μ M) using antibodies against P-ERK1/2, P-Rb, survivin, RelB, and HSP60 as loading control.
- F, G Immunoblot analysis of protein extracts obtained from SKMEL5 (F) or MM099 (G) cells plated on FRC- or MAF-derived ECMs and treated with 5 μ M BRAFi in combination or not with DDR1-IN-1 (5 μ M for SKMEL5 and 3 μ M for MM099) or 10 μ M NIK inhibitor (NIKi) for 96 h. Antibodies against P-ERK1/2, ERK2, P-Rb, Rb, survivin, caspase-3, cleaved caspase-3, RelB, p100/p52, and HSP60 as loading control were used.

Source data are available online for this figure.

MMDR involves a targetable pro-survival NIK/IKK α /NF- κ B2 pathway

Finally, we wished to better characterize at the molecular level the MMDR process that is promoted by collagen receptors DDR1 and DDR2. To identify MMDR-related signaling pathways triggered by their tyrosine kinase activity, we performed a phospho-kinase screening with protein extracts from melanoma cells cultured on fibroblast-derived 3D ECMs or plastic, in the presence of BRAFi. Unfortunately, this approach did not reveal any significantly augmented kinase activity or increased phosphorylation of kinase substrates (Appendix Fig S7A and B). Moreover, consistent with the results of the phospho-kinase screening, using immunoblot analysis, we did not observe by immunoblot analysis any changes in the phosphorylation of the AKT survival pathway in melanoma cells cultured under MMDR conditions (Appendix Fig S7C). On the contrary, compared to siCTRL cells, biochemical analysis of DDR-silenced melanoma cells revealed that the concomitant depletion of the two receptors decreased the expression of RelB, NF- κ B2 precursor protein p100, and NF- κ B2 p52 processed form, in SKMEL5 and MM099 cells cultured in MMDR conditions, following exposure to BRAFi alone or in combination with MEKi (Fig 8A and B). A similar decrease in RelB and p100 was observed in DDR-depleted 1205Lu cells, following treatment with targeted agents (Fig EV5A). Consistent with these results, pharmacological inhibition of DDR using imatinib that impaired melanoma MMDR by triggering cell cycle arrest and apoptosis decreased in a time-dependent manner the expression of RelB in 1205Lu cells cultured in MMDR conditions (Fig EV5B).

RelB and p52 are components of the non-canonical NF- κ B2 pathway (Taniguchi & Karin, 2018), which is activated by the upstream kinases NIK (NF- κ B-inducing kinase) and IKK α (I κ B kinase) (Fig 8C). Interestingly, levels of RelB and p52 were found to be elevated in melanoma cells cultured on fibroblast-derived ECMs compared to plastic and collagen-coated dishes (Fig 8D). Using a pan- IKK inhibitor BMS-345541 (Figs 8E and EV5C and D) and a recently developed NIK inhibitor (NIKi; Mondragon *et al*, 2019; Figs 8F and G, and EV5E), we confirmed the implication of the NF- κ B2 pathway in MMDR, as illustrated by decreased cell cycle markers (pRb and survivin) and increased caspase-3 cleavage, in BRAFi-treated melanoma cells cultured on FRC- or MAF-derived ECMs. Comparable decreased levels of p52 and RelB, as well as cell cycle markers, were observed following pharmacological targeting of DDR and NIK in MMDR conditions (Figs 8F and G, and EV5E). Together,

our findings suggest that melanoma cell adaptation to oncogenic MAPK pathway inhibition involves the interaction of tumor cells with the mesenchymal stroma enriched in fibrillar collagens, thereby promoting DDR-dependent activation of the NF- κ B2/RelB pathway (Fig 9).

Discussion

Preventing melanoma resistance and relapse to targeted therapy remains a significant challenge for successful disease management. Emerging evidence suggests that stromal components of the tumor microenvironment, including the ECM, play a key role in establishing resistant niches by allowing melanoma cells to rapidly adapt and tolerate therapeutic drugs, before mutation-driven resistance mechanisms are acquired (Meads *et al*, 2009; Smith *et al*, 2016; Rambow *et al*, 2019). Here, we describe a novel mechanism of adaptation and tolerance to oncogenic BRAF pathway inhibition, which involves the dynamic interaction of melanoma cells with the ECM. When comparing cell-derived matrices produced by normal HDF, FRC, and MAF, we found that depending on fibroblast origin, properties of experimentally derived ECMs differ remarkably. MAF-derived ECMs exhibit a higher level of fiber organization and increased stiffness compared to ECMs generated by normal dermal fibroblasts (HDF). This is in agreement with what has been previously demonstrated by others (Gopal *et al*, 2017; Kaukonen *et al*, 2017). Interestingly, we observed that FRC, which are resident lymph node fibroblasts, harbor some phenotypic and functional properties similar to MAF such as myofibroblast-like properties. In this regard, FRC produce and remodel a stiff ECM enriched in fibrillar collagens. Consistent with this, we show that similar to MAF-derived ECM, the ECM generated by FRC provides melanoma cells with increased protection from targeted drugs, compared to ECMs generated from HDF. However, it is important to note that in contrast to classic 2D culture conditions, HDF-derived ECMs can confer protection against BRAF inhibition, indicating that MMDR is dependent on structural 3D ECM organization. Importantly, MMDR is described in three different BRAF mutant melanoma cells, regardless of their transcriptional phenotypic MITF/AXL signature.

Functionally, we demonstrate that collagen receptors DDR1 and DDR2 mediate MMDR to BRAF/MEK inhibitor therapy through a pro-survival NIK/IKK α /NF- κ B2 pathway. We show that DDR knock-down or the inhibition of their catalytic activity impairs drug

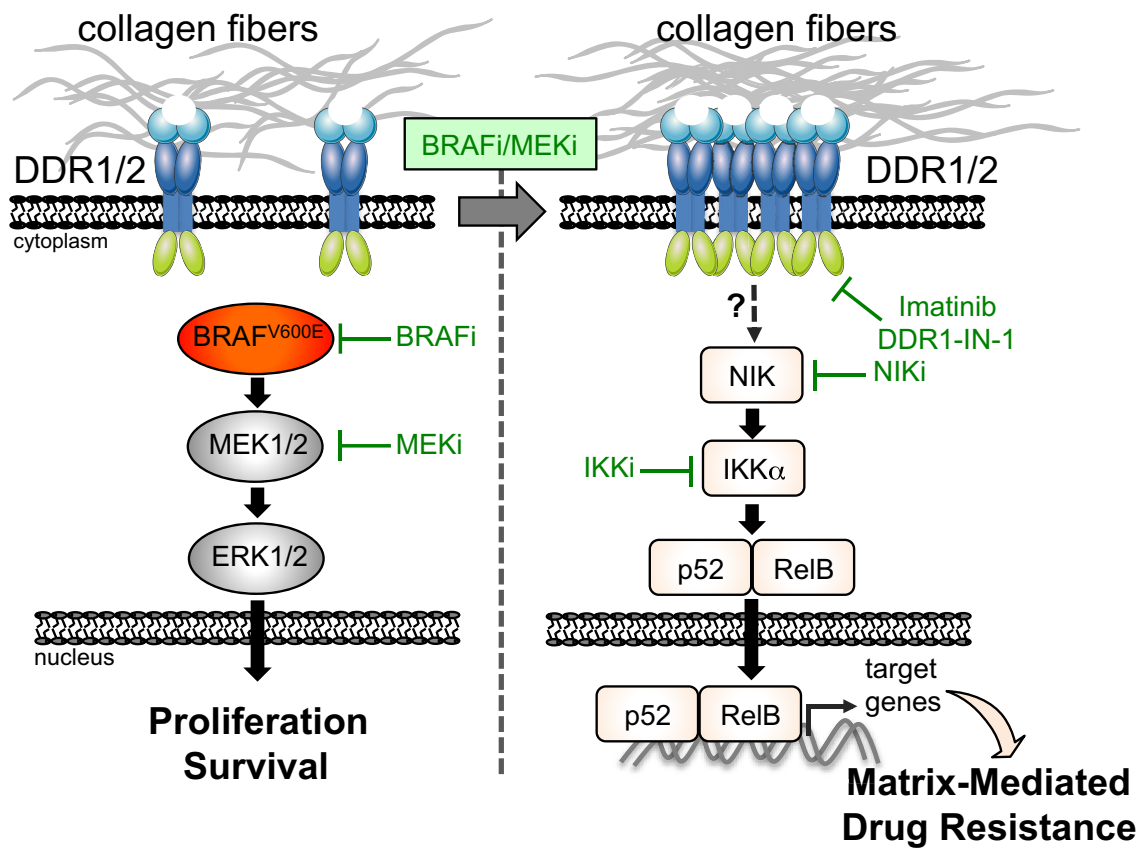


Figure 9. Model of DDR-dependent matrix-mediated drug resistance (MMDR) to MAPK-targeting therapies in melanoma.

BRAF-mutated melanoma cells adapt to BRAF/MEK inhibition by turning on a drug-tolerant pathway that is initiated by collagen-rich environments interacting with cancer cell DDR. Clustered DDR activates the non-canonical NF- κ B2 (p52/RelB) pathway that is therapeutically targetable with clinically approved DDR inhibitor such as imatinib or with preclinically tested NIK inhibitors.

tolerance that is promoted by MAF- or FRC-derived ECM and induces melanoma cell death. DDR1 and DDR2 are both expressed at different levels in the skin (Cario, 2018), particularly in the epidermis from which melanoma originates following the malignant transformation of melanocytes. Overlapping functions have been attributed to DDR1 and DDR2 in melanoma with regard to cancer cell growth and invasiveness. A recent study correlated high DDR1 expression in melanoma lesions with poor prognosis and showed that DDR1 controls melanoma cell invasion and survival (Reger de Moura *et al*, 2019). Other studies have reported that DDR2 depletion in melanoma cell lines reduced their invasive and metastatic abilities (Badiola *et al*, 2011; Poudel *et al*, 2015). Consistently, we observed augmented expression of the two receptors during the malignant transition from benign melanocytic lesions to metastatic melanoma and that their expression is linked with therapy-resistant melanoma cell populations. Our data therefore suggest that the function of DDR1 and DDR2 also overlaps during the response to BRAF^{V600}-targeted therapy. Accordingly, knockdown of both receptors is required to fully prevent MMDR to oncogenic BRAF pathway inhibition.

Collagen abundance has recently been identified as an important contributor to melanoma cell phenotype switching through lineage-specific microenvironment sensing (Miskolczi *et al*, 2018). Herein, we provide evidence for a role of collagen-rich matrices during the

adaptive phase of tolerance to targeted therapies. Interestingly, β 1 integrin, another collagen receptor that plays a major role in EMDR (Seguin *et al*, 2015), has also been linked to adaptive responses to BRAF inhibition via fibronectin-mediated activation of FAK, leading to MAPK pathway reactivation (Fedorenko *et al*, 2015; Hirata *et al*, 2015). Contrary to β 1 integrin, engagement of DDR by collagens mediates drug tolerance in the absence of MAPK/ERK pathway reactivation. This suggests that DDR participate in the early response to BRAF inhibition through a pathway distinct from that of β 1 integrin. Additionally, we show that fibroblast-derived ECMs promote phospho-DDR1/2 clustering into linear membrane structures aligned with collagen and resembling those described by others (Agarwal *et al*, 2007; Corcoran *et al*, 2019; Yeung *et al*, 2019). Importantly, receptor linear clustering is enhanced upon melanoma cell treatment with targeted therapies, thus making the involvement of this process during the early phase of drug adaptation highly probable. In addition, linear clustering of phospho-DDR upon BRAF pathway inhibition is favored on MAF- and FRC-derived ECMs compared to HDF-derived ECM, correlating with the topological organization of collagen fibers and their drug-protective effect. The exact mechanism underlying the induction of DDR clustering following MAPK pathway inhibition is, however, unknown.

Biochemical studies revealed that fibroblast-derived matrices enhance the activation of the non-canonical NF- κ B2 pathway that

account for most of the melanoma cell tolerance to BRAF/MEK inhibition. The NF- κ B/p52/RelB pathway represents a major alternative route of NF- κ B signaling (Taniguchi & Karin, 2018), which has been involved in drug resistance in myeloma (Landowski *et al*, 2003) and prostate cancer (Nadiminty *et al*, 2013). In melanoma, the NF- κ B2 pathway is upregulated compared to melanocytes and prevents melanoma senescence (De Donatis *et al*, 2016). In this study, we demonstrate that suppression of DDR signaling impairs MMDR by reducing NF- κ B2/p52/RelB expression. In addition, inhibition of NIK or IKK α , two upstream activators of the NF- κ B2 pathway (Taniguchi & Karin, 2018), also abrogates ECM-mediated resistance to BRAF pathway inhibition. Further supporting a potential role for the NF- κ B2 pathway in melanoma resistance to targeted therapy is the observation that the drug-resistant undifferentiated and neural crest-like subpopulations display a strong enrichment for the NIK/NF- κ B signaling pathway (Tsoi *et al*, 2018). Precisely how DDR interact with the NIK/IKK α /NF- κ B2 pathway remains to be determined. The adaptive response of melanoma cells to BRAF inhibition implicates force-induced actomyosin cytoskeletal remodeling (Kim *et al*, 2016; Girard *et al*, 2020; Orgaz *et al*, 2020). In addition, DDR1 clustering and collagen mechanical reorganization have been shown to involve interactions with myosin IIA, a key component of the actomyosin network (Coelho *et al*, 2017). In cancer cells, the classical NF- κ B pathway is activated by mechanical cues and RhoA-ROCK-myosin II signaling (Sero *et al*, 2015). We can therefore speculate that BRAFi/MEKi-driven cytoskeletal reorganization and DDR linear clustering along with collagen fibrils regulate the NIK/IKK α /NF- κ B2 pathway by increasing actomyosin tension. Another possibility is the recruitment of NIK/IKK α to the DDR signaling platforms, leading to their enzymatic activation, p52/RelB regulation, and MMDR.

Our recent report revealed that increased collagen deposition and tumor stiffening is an early response to BRAF inhibition to create a drug-protective niche (Girard *et al*, 2020). In this study, DDR inhibition by the clinically approved TKI imatinib improved the action of BRAFi on melanoma treatment by delaying tumor relapse, normalizing the collagen network, and increasing mouse survival. Thus, this combination strategy could be effective in a clinical application as it allows the suppression of the stromal fibrotic-like reaction induced by oncogenic BRAF pathway inhibition and prevents tumor relapse. Our findings support a model in which BRAF-targeted drugs fuel a self-feeding mechanism involving collagen-bound DDR signaling platforms, responsible for collagen network remodeling and drug tolerance. Another issue highlighted by our *in vivo* drug response melanoma model is the possible implication of stromal DDR in the therapeutic response. Consistent with this, a major role of CAF-derived DDR2 in collagen fiber organization and breast cancer metastasis has been reported (Corsa *et al*, 2016). DDR signaling might therefore influence both cancer and stromal cells during tumor adaptation to BRAF inhibition.

Our work adds to the emerging notion that DDR are becoming attractive targets in anti-cancer therapies. Inhibiting DDR1 or DDR2 with nilotinib (Jeitany *et al*, 2018), dasatinib (Hammerman *et al*, 2011; von Massenhausen *et al*, 2016), or other non-approved inhibitors (Ambrogio *et al*, 2016; Grither & Longmore, 2018) was shown to decrease tumorigenicity, invasion, or metastasis of several carcinomas (Corsa *et al*, 2016). Importantly, a recent study in melanoma reported that targeting DDR2 with dasatinib enhances tumor response to anti-PD-1 immunotherapy (Tu *et al*, 2019). Together,

this study and our work point to the critical role of collagen receptors DDR in regulating the immune and mesenchymal stroma and the response to current therapies in melanoma.

In summary, our findings reveal that interaction of matrix collagen fibers with DDR favors the emergence of drug-tolerant melanoma cells, during the initial phase of adaptation to MAPK-targeting therapies. We also provide evidence that targeting MMDR with clinically approved DDR inhibitors may represent an attractive salvage strategy to overcome resistance to oncogenic BRAF inhibition. This combinatorial approach may thus be beneficial for melanoma patients treated with targeted therapies.

Materials and Methods

Melanoma cells, reagents, and antibodies

Melanoma cell lines were obtained as previously described (Tichet *et al*, 2015; Didier *et al*, 2018; Rathore *et al*, 2019). Isogenic pairs of vemurafenib-sensitive (P) and vemurafenib-resistant (R) cells (M229, M238, M249) were provided by R.S. Lo (Nazarian *et al*, 2010). The isogenic pair of vemurafenib-sensitive (UACC62P) and vemurafenib-resistant (UACC62R) cells was provided by R. Neubig (Misek *et al*, 2020). Short-term cultures of patient melanoma cells were kindly provided by J.C. Marine and are described elsewhere (Verfaillie *et al*, 2015; Wouters *et al*, 2020). Melanoma cells were cultured in Dulbecco's modified Eagle's medium (DMEM) supplemented with 7% fetal bovine serum (FBS) (HyClone) and 1% penicillin/streptomycin solution. Cell lines were used for experiments within 6 months of thawing. To guarantee cell line authenticity, cells were expanded and frozen at the lowest possible passages and used for a limited number of passages after thawing. Cells were routinely tested for the expression of melanocyte lineage proteins such as MITF. All cell lines were routinely tested for the absence of mycoplasma using PCR. For live imaging and red nuclear labeling, 1205Lu cells were transduced with NuLight Red Lentivirus Reagent (Essen Bioscience) and selected with puromycin (1 μ g/ml, Sigma-Aldrich).

Culture reagents were purchased from Thermo Fisher Scientific. BRAFi (PLX4032, vemurafenib), MEKi (GSK1120212, trametinib, and GDC-0973/RG7420, cobimetinib), dual BRAFi/MEKi (RO5126766), DDR1-IN-1, nilotinib, and IKK inhibitor, BMS-345541, were obtained from Selleckchem. Imatinib mesylate was purchased from Enzo Life Sciences. The NIK inhibitor was described before (Mondragon *et al*, 2019). FAK inhibitor PF573228 was from Tocris Bioscience. An equal amount of DMSO was used as the vehicle control. Tissue culture grade collagen I (#A1064401) used for coating wells and plates was obtained from Thermo Fisher Scientific. Collagen I (#354249) used for 3D applications was obtained from Corning. Matrigel (#E1270) and all other reagents were obtained from Sigma-Aldrich unless otherwise stated. β 1 integrin blocking antibody (clone AIIB2) and the control isotype were purchased from Merck Millipore. Information on antibodies used in this study is provided in Appendix Table S1.

Isolation and culture of primary fibroblasts and MAFs

Human dermal fibroblasts were isolated and maintained as previously described (Robert *et al*, 2006). Human lymphatic fibroblasts

(FRC#2 and FRC#5) were purchased from ScienCell Research Laboratories. Metastatic melanoma clinical specimens were obtained with written informed consent from each patient, and studies were approved by the hospital ethics committee (Nice Hospital Center and University Côte d'Azur). The experiments conformed to the principles set out in the WMA Declaration of Helsinki and the Department of Health and Human Services Belmont Report. Briefly, the tissue sample was cut into small pieces and digested using collagenase/dispase. Following filtration of the large debris, the solution was serially centrifuged and the final pellet was resuspended in DMEM supplemented with 10% FBS and seeded in a tissue culture dish. After 30 min, the fibroblasts adhered to the dish, while other cellular types remained in suspension. Verification of MAF was determined by flow cytometry using CAF markers such as $\beta 1$ integrin, PDGFR β , FAP α , and α SMA.

Fibroblasts were cultured in fibroblast medium (ScienCell) supplemented with 10% FBS, 1% fibroblast growth supplement (FGS), and 1% penicillin/streptomycin solution. All experiments were performed with fibroblasts until passage 10.

Fibroblast-derived 3D ECM and MMDR assay

3D de-cellularized ECMs were generated as previously described (Beacham *et al.*, 2007). Briefly, fibroblasts were seeded in gelatin-coated tissue culture dishes, cultured for 8 days in a complete medium, and treated with 50 μ g/ml ascorbic acid every 48 h. Cells were then washed with PBS, and ECMs were de-cellularized using a prewarmed extraction buffer for 2 min (PBS 0.5% Triton X-100, 20 mM NH₄OH). Matrices were then gently washed several times with PBS.

For MMDR assays, melanoma cells were seeded on top of the de-cellularized 3D ECMs for 48 h at 37°C in 5% CO₂, and cultured in a complete medium for a further 96 h in the presence of the various inhibitors, as indicated in the figure legends. Cells were detached and fixed in 70% ethanol or lysed in lysis buffer for cell cycle and immunoblot analysis, respectively.

Matrix-remodeling assay

5×10^4 fibroblasts were embedded in 100 μ l of collagen I/Matrigel mix (final concentration of collagen I: 4 mg/ml and Matrigel: 2 mg/ml), seeded in a glass-bottom 96-well plate (MatTek), and maintained in DMEM supplemented with 10% FBS for 6 days. The gel area was measured using ImageJ software, and the gel contraction was calculated using the formula $100 \times (\text{well diameter} - \text{gel diameter}) / \text{well diameter}$ as previously described (Albregues *et al.*, 2014).

RNAi studies

Non-targeting control, DDR1#1 (VHS50139), DDR1#2 (HSS187878), DDR2#1 (HSS107350), and DDR2#2 (HSS107352), and FAK (PTK2) siRNA duplexes were purchased from Thermo Fisher Scientific. Transfection of siRNA was carried out using Lipofectamine RNAiMAX (Thermo Fisher Scientific), at a final concentration of 50 nM. Unless stated otherwise, cells were assayed at 2 or 4 days post-transfection.

Immunoblot and immunoprecipitation

Whole-cell lysates were prepared using lysis buffer containing 50 mM HEPES, 150 mM NaCl, 1.5 mM MgCl₂, 1 mM EDTA, 10%

glycerol, and 1% Triton X-100 supplemented with protease and phosphatase inhibitors (Pierce) and briefly sonicated. Proteins were separated using SDS-PAGE and were transferred onto PVDF membranes (GE Healthcare Life Sciences) for immunoblot analysis. Membranes were incubated with the primary antibody overnight, washed, and then incubated with the peroxidase-conjugated secondary antibody. Antibodies and working dilution used are listed in Appendix Table S1. Blots were developed with a chemiluminescence system (GE Healthcare Life Sciences).

For immunoprecipitation (IP) assays, cells treated with 10 μ g/ml of collagen I for 18 h with the indicated inhibitors were lysed as described above, then incubated overnight at 4°C with rocking in lysis buffer containing Protein G Sepharose beads (Merck) and an antibody directed against DDR2. Beads were then washed 3 times with 20 mM HEPES, 150 mM NaCl, 10% glycerol, and 0.1% Triton X-100 supplemented with protease and phosphatase inhibitors. IP products were separated using SDS-PAGE and subjected to immunoblot analysis.

Proliferation assay

Real-time analysis of cell growth was carried out using the IncuCyte™ ZOOM imaging system (Essen Bioscience). 1205Lu melanoma cells stably expressing the nuclear fluorescent label red NuLight reagent were seeded in triplicate in a complete medium (15×10^3 cells/well in 12-well plates) on fibroblast-derived 3D ECM, in collagen I-coated wells, or in uncoated plastic wells and treated with the indicated drugs. Phase-contrast and red immunofluorescent images were taken every 6 h over a 5-day period (4 images per well at $\times 4$ magnification). Cell proliferation was quantified by counting the number of fluorescent nuclei over time, which was calculated as the cell growth rate. Growth curves were generated using the GraphPad Prism 8 software. Alternatively, cell proliferation was analyzed by counting cells with Hoechst-stained nuclei.

Flow cytometry

Cell cycle profiles were determined using flow cytometry analysis of propidium iodide (PI)-stained cells as previously described (Didier *et al.*, 2018). Melanoma cells were cultured on top of fibroblast-derived ECMs, collagen I-coated wells, or uncoated plastic wells and were treated with the indicated drugs for 96 h. Cells were then washed, fixed in 70% ethanol, and incubated at -20°C for 24 h. Finally, cells were stained for 20 min at 37°C in buffer containing 40 μ g/ml PI and 20 μ g/ml ribonuclease A. Cell cycle profiles were collected using the FACSCanto II (Becton Dickinson). Cell death was evaluated following staining with Annexin V/PI (eBioscience) and analyzed by flow cytometry as described (Didier *et al.*, 2018).

Immunofluorescence and microscopy

Cells were grown on type I collagen- (0.14 mg/ml) or fibroblast-derived ECM-coated glass coverslips. Following BRAFi or BRAFi+MEKi treatment, cells were rinsed with PBS, fixed in 4% paraformaldehyde (PFA), and incubated for 1 h in PBS containing 10% normal goat serum (Cell Signaling), and then incubated overnight with the indicated primary antibodies that were diluted in PBS containing 2% normal goat serum. F-actin was stained with Alexa

Fluor 488 phalloidin (1:100; Thermo Fisher Scientific), and nuclei were stained with DAPI. Following incubation with Alexa Fluor-conjugated secondary antibodies, coverslips were mounted in ProLong antifade mounting reagent (Thermo Fisher Scientific). Images were captured using a wide-field microscope (Leica DM5500B, at $\times 63$ magnification). Cell area and globular versus linear clusters of cells ($n > 20$) were determined and quantified using ImageJ software. For quantification of globular versus linear clusters of phospho-DDR1/2, a “subtract background” function of ImageJ was applied to all images. In order to quantify clusters, the IsoData threshold was used. Clusters with circularity 0.3–1 were defined as “globular” and clusters with circularity 0 to 0.29 as “linear”. Following fixation and incubation with primary antibodies and Alexa Fluor-conjugated secondary antibodies, de-cellularized matrices on coverslips were mounted in ProLong antifade reagent. Images were captured using a wide-field microscope (Leica DM5500B, at $\times 40$ magnification). The orientation of fibronectin and collagen fibers was assessed in the immunofluorescence images using ImageJ software. Data were plotted as frequency of distribution. For co-localization analyses of collagen 1 and phospho-DDR1/2, an anti-collagen type I mouse monoclonal antibody (Sigma, C2456) was used.

Cleaved caspase-3 and Ki67 stainings were assessed on 5- μ m frozen sections of cell-derived melanoma xenografts. Samples were fixed for 30 min with 4% PFA in PBS, rehydrated for 10 min in Tris 0.1 M, permeabilized in Tris 0.1 M + 1% Triton for 1 h, and then blocked for 1 h in Tris 0.1 M containing 1% BSA, 0.3% Triton, and anti-CD16/CD32 (FC Block, 1/100). Antibodies were diluted in Tris 0.1 M containing 1% BSA and 0.3% Triton and incubated overnight at 4°C. Following several washes with Tris 0.1 M, bound antibodies were detected using Alexa Fluor 488- or Alexa Fluor 594-conjugated secondary antibody. Images were captured using a wide-field microscope (Leica DM5500B, at $\times 40$ magnification).

Mass spectrometry analysis

Proteomic analysis of de-cellularized 3D ECMs was performed as described (Gopal *et al*, 2017). Briefly, ECM proteins were solubilized in urea, reduced, and alkylated, and proteins were digested with PNGase F (New England BioLabs), endoproteinase Lys-C (Promega), and high-sequencing-grade trypsin. Each sample was reconstituted in 0.1% trifluoroacetic acid (TFA) 2% acetonitrile and analyzed using liquid chromatography (LC)–tandem mass spectrometry (MS/MS) in an LTQ Orbitrap Velos (Thermo Electron, Bremen, Germany) online with a nanoLC Ultimate 3000 chromatography system (Dionex). Protein identification and estimation of abundance were determined using raw LC Orbitrap MS data that were processed using the MASCOT search engine (version 2.4.1). Spectra were searched against a SwissProt Human database. The protein abundance was calculated using the iBAQ score and represented as molar percent.

Phospho-kinase profiling

Phospho-kinase screening was performed using a phospho-kinase array (Proteome Profiler Human Phospho-Kinase Array #ARY003B; R&D Systems) according to the manufacturer's instructions. After cell extraction, 600 μ g of protein was added per sample. Array spots were analyzed using ImageJ software.

Atomic force microscopy

Elastic properties of fibroblast-derived 3D ECMs were analyzed by AFM using a BioScope Catalyst operating in Point and Shoot (Bruker Nano Surfaces), coupled with an inverted optical microscope (Leica DMI6000B, Leica Microsystems Ltd.). The apparent Young's modulus (Eapp) was measured on unfixed ECM using a silicon nitride tip (40 nm of diameter) mounted on a cantilever with a nominal spring constant of 0.03 N/m (MLCT-D, Bruker). The force–distance curves were collected using a velocity of 4.5 μ m/s, in relative trigger mode, and by setting the trigger threshold to 1 nN. Each point represents a specific Young's modulus obtained by fitting the corresponding individual force curve acquired on a determined point of the sample. Eapp values were represented as scatter dot plot using GraphPad Prism software.

Cell line-derived xenograft (CDX) tumor models

Mouse experiments were carried out in accordance with the Institutional Animal Care and the local ethics committee (CIEPAL-Azur agreement NCE/2018-483). 6-week-old female athymic nude nu/nu mice were purchased from Janvier Labs (France) and maintained under specific pathogen-free conditions in our accredited animal housing facility. 1×10^6 1205Lu melanoma cells were subcutaneously implanted into both flanks. The tumor was measured with a caliper, and the volume was calculated using the formula: $V = \text{width} \times \text{length}^2 \times 0.5$. When the tumor reached 75 mm³, mice were randomly grouped into control and test groups. Vemurafenib (35 mg/kg) and imatinib mesylate (75 mg/kg) were delivered (alone or in combination) intraperitoneally three times per week. Mice in the control group were treated with vehicle alone. Mice were treated for 30 days and followed for up to 50 days or until tumors reached a predefined volume (1,000 mm³). Once the animals were sacrificed, tumors were dissected, weighed, and snap-frozen in liquid nitrogen in an optimal cutting temperature compound (OCT; Tissue-Tek) (Gentaur). The sections were processed as described above and analyzed using immunofluorescent microscopy or formalin-fixed and paraffin-embedded for picrosirius red staining or SHG analysis.

Fibrillar collagen imaging

Collagen in de-cellularized 3D ECMs or in paraffin-embedded melanoma tissues was stained with picrosirius red using standard protocols. Tumor sections were analyzed using polarized light microscopy as previously described (Rich & Whittaker, 2005). Images were acquired under polarized illumination using a light transmission microscope (Zeiss PALM, at $5\times$ magnification). Fiber thickness was analyzed according to the change in polarization color. Birefringence hue and amount were quantified as a percent of total tissue area using ImageJ software. SHG imaging of paraffin-embedded melanoma tissues was recorded on a Zeiss 510 NLO microscope (Carl Zeiss Microscopy) with the Mai Tai HP DeepSee (Newport Corporation) and 360- to 440-nm band-pass filter.

Tissue microarray analysis

Immunohistochemistry analysis of DDR1 and DDR2 expression was assessed on TMA sections (US Biomax, #ME1004h) using

The paper explained

Problem

Despite novel targeted therapies for BRAF mutant advanced melanoma, therapy-driven resistance remains a major hurdle that limits patient benefit. Emerging evidence supports that tumor microenvironment components such as the surrounding extracellular matrix play a key role in creating resistant niches by allowing melanoma cells to rapidly adapt and tolerate anti-cancer drugs. However, how the extracellular matrix contributes to drug resistance remains poorly understood. Thus, a better understanding of the complexities of this tumor–host interaction may offer new therapeutic strategies to obviate melanoma resistance to treatment targeting the BRAF oncogenic pathway.

Results

To model the contribution of the extracellular matrix in melanoma cell response to BRAF-targeted therapy, we generated cell-derived 3D matrices from fibroblasts isolated from patient-derived biopsies and analyzed their effectiveness to protect melanoma cells against the anti-proliferative effect of oncogenic BRAF inhibition. We demonstrate that melanoma cells cultured on matrices adapt to BRAF/MEK inhibition by turning on a drug-tolerant pathway that is initiated by the tyrosine kinase receptors for collagens DDR1 and DDR2. Clustered DDR activate a non-canonical NF- κ B2 (p52/RelB)-resistant pathway that is therapeutically targetable with clinically approved compounds such as imatinib or with a preclinically tested inhibitor of the NIK/NF- κ B2 pathway. In melanoma cell-derived xenografts, targeting DDR by imatinib enhances BRAF inhibitor efficacy, counteracts therapy-induced fibrillar collagen remodeling, and delays tumor relapse.

Impact

This study outlines the critical interaction between melanoma cells and the extracellular matrix in mediating tolerance to BRAF/MEK inhibitor therapy and reveals that targeting DDR signaling may represent an attractive salvage strategy to overcome collagen-mediated drug resistance. It provides a rationale for designing clinical trials with clinically approved drugs such as imatinib in BRAF mutant melanoma patients treated with targeted therapies.

VECTASTAIN Elite ABC Kit (Vector Laboratories) with the DAB reagent (Vector Laboratories) and counterstained with hematoxylin (Fisher Scientific), according to the manufacturer's instructions. Images were captured using a bright-field microscope (Nikon, at 20 \times magnification). Histological scoring of the samples was performed in a blinded fashion.

Analysis of gene expression from public databases

Publicly available gene expression datasets of human melanoma cell lines were used to analyze *DDR1*, *DDR2*, *MITF*, *AXL*, and *SOX10* levels according to the differentiation status. Cell states were classified into four differentiation states (undifferentiated, neural crest-like, transitory, and melanocytic) as previously described (Tsoi *et al*, 2018) and using GSE80829 and <https://systems.crump.ucla.edu/dediff/>. *DDR1*, *DDR2*, *MITF*, and *AXL* expression was analyzed in human melanoma samples within the Mannheim (GSE4843), Philadelphia (GSE4841), and Zurich (GSE4840) cohorts (Widmer *et al*, 2012). Proliferative (MITF^{high} AXL^{low}) and invasive (MITF^{low} AXL^{high}) melanoma subgroups were defined as previously described (Widmer *et al*, 2012; Rathore *et al*, 2019). Genomic alterations in *DDR1* and *DDR2* from the skin melanoma TCGA database were retrieved using cBioPortal

(<http://www.cbioportal.org/>). Correlation between *DDR1* genomic alterations and expression and the activity ($-\log_{10}$ [IC50 M]) of BRAFi (dabrafenib, vemurafenib) and MEKi (trametinib) were performed across the GDSC (Genomic of Drug Sensitivity in Cancer) melanoma cell line pharmacogenomic data using CellMinerCDB (<https://discover.nci.nih.gov/cellminercdb>; Luna *et al*, 2021).

Statistical analysis

Unless otherwise stated, all experiments were repeated at least three times and representative data/images are shown. Statistical data analysis was performed using GraphPad Prism 8 software. The unpaired two-tailed Mann–Whitney test was used for statistical comparisons between two groups. The Kruskal–Wallis test with the indicated post-tests or two-way ANOVA test with Sidak's, Dunnett's, or Tukey's post-tests was used to compare three or more groups. A chi-square test was performed for statistical analysis of tissue microarray stainings. A log-rank (Mantel–Cox) test was applied to the Kaplan–Meier survival curves. Data represent biological replicates (n) and are depicted as mean values \pm SEM as indicated in the figure legends.

Data availability

The mass spectrometry proteomics data have been deposited to the ProteomeXchange Consortium (<http://www.proteomexchange.org>) via the PRIDE partner repository with the dataset identifier PXD026645 (<http://www.ebi.ac.uk/pride/archive/projects/PXD026645>).

Expanded View for this article is available online.

Acknowledgments

We thank Roger Lo for the M229P/R, M238P/R, and M249P/R melanoma cells, Chris Marine and Ghanem Ghanem for the short-term cultured melanoma cells and Richard Neubig for the UACC62 parental and resistant melanoma cells. We acknowledge Maeva Gesson and Marie Irondele from the C3M imaging facility for their helpful advice. We thank the C3M animal facility and Cédric Matthews for the SHG microscopy analysis (IBDM imaging platform, AMU-Marseille). We also thank Ana Popovic for critical reading of the manuscript. This work was supported by funds from the: Institut National de la Santé et de la Recherche Médicale (Inserm), Ligue Contre le Cancer, Institut National du Cancer (INCA_12673), ITMO Cancer Aviesan (Alliance Nationale pour les Sciences de la Vie et de la Santé, National Alliance for Life Science and Health) within the framework of the Cancer Plan, and the French Government (National Research Agency, ANR) through the "Investments for the Future" LABEX SIGNALIFE: program reference # ANR-11-LABX-0028-01. We also thank the PiCSL-FBI platform (IBDM, AMU-Marseille), a member of France BioImaging, supported by the "Investments for the Future" (ANR-10-INBS-04). The financial contribution of the Conseil général 06, Canceropôle Provence Alpes Côte d'Azur, and Région Provence Alpes Côte d'Azur to the C3M is also acknowledged. I.B. was a recipient of a doctoral fellowship from Ligue Contre le Cancer.

Author contributions

ST-D and MD designed the study, analyzed and interpreted data, ensured financial support, and wrote the paper with inputs from IB, AP, VP, and CAG. IB performed the majority of the experiments and analyzed the data with the help of ML, AC, AM, SD, MO, CR, VP, AP, and CAG. FL performed the flow

cytometry analyses. SP performed the AFM analyses. SA performed the mass spectrometry analyses. CG and TP contributed to reagents and expertise.

Conflict of interest

T.P. is the co-founder of Yukin Therapeutics. The remaining authors declare that they have no conflict of interest.

References

- Agarwal G, Mihai C, Iscru DF (2007) Interaction of discoidin domain receptor 1 with collagen type 1. *J Mol Biol* 367: 443–455
- Albregues J, Bourget I, Pons C, Butet V, Hofman P, Tartare-Deckert S, Feral CC, Meneguzzi G, Gaggioli C (2014) LIF mediates proinvasive activation of stromal fibroblasts in cancer. *Cell Rep* 7: 1664–1678
- Ambrogio C, Gómez-López G, Falcone M, Vidal A, Nadal E, Crosetto N, Blasco RB, Fernández-Marcos PJ, Sánchez-Céspedes M, Ren X et al (2016) Combined inhibition of DDR1 and Notch signaling is a therapeutic strategy for KRAS-driven lung adenocarcinoma. *Nat Med* 22: 270–277
- Badiola I, Villace P, Basaldua I, Olosa E (2011) Downregulation of discoidin domain receptor 2 in A375 human melanoma cells reduces its experimental liver metastasis ability. *Oncol Rep* 26: 971–978
- Beacham DA, Amatangelo MD, Cukierman E (2007) Preparation of extracellular matrices produced by cultured and primary fibroblasts. *Curr Protoc Cell Biol* Chapter 10: Unit 10 19
- Cario M (2018) DDR1 and DDR2 in skin. *Cell Adh Migr* 12: 386–393
- Coelho NM, Arora PD, van Putten S, Boo S, Petrovic P, Lin AX, Hinz B, McCulloch CA (2017) Discoidin domain receptor 1 mediates myosin-dependent collagen contraction. *Cell Rep* 18: 1774–1790
- Corcoran DS, Juskaite V, Xu Y, Gorlitz F, Alexandrov Y, Dunsby C, French PMW, Leitinger B (2019) DDR1 autophosphorylation is a result of aggregation into dense clusters. *Sci Rep* 9: 17104
- Corsa C, Brenot A, Grither W, Van Hove S, Loza A, Zhang K, Ponik S, Liu Y, DeNardo D, Eliceiri K et al (2016) The action of discoidin domain receptor 2 in basal tumor cells and stromal cancer-associated fibroblasts is critical for breast cancer metastasis. *Cell Rep* 15: 2510–2523
- Cukierman E, Pankov R, Stevens DR, Yamada KM (2001) Taking cell-matrix adhesions to the third dimension. *Science* 294: 1708–1712
- Day E, Waters B, Spiegel K, Alnadaf T, Manley PW, Buchdunger E, Walker C, Jarai G (2008) Inhibition of collagen-induced discoidin domain receptor 1 and 2 activation by imatinib, nilotinib and dasatinib. *Eur J Pharmacol* 599: 44–53
- De Donatis GM, Pape EL, Pierron A, Cheli Y, Hofman V, Hofman P, Allegra M, Zahaf K, Bahadoran P, Rocchi S et al (2016) NF- κ B2 induces senescence bypass in melanoma via a direct transcriptional activation of EZH2. *Oncogene* 35: 2735–2745
- Didier R, Mallavialle A, Ben Jouira R, Domdom MA, Tichet M, Auberger P, Luciano F, Ohanna M, Tartare-Deckert S, Deckert M (2018) Targeting the proteasome-associated deubiquitinating enzyme USP14 impairs melanoma cell survival and overcomes resistance to MAPK-targeting therapies. *Mol Cancer Ther* 17: 1416–1429
- Druker BJ, Sawyers CL, Kantarjian H, Resta DJ, Reese SF, Ford JM, Capdeville R, Talpaz M (2001) Activity of a specific inhibitor of the BCR-ABL tyrosine kinase in the blast crisis of chronic myeloid leukemia and acute lymphoblastic leukemia with the Philadelphia chromosome. *N Engl J Med* 344: 1038–1042
- Fedorenko IV, Wargo JA, Flaherty KT, Messina JL, Smalley KSM (2015) BRAF inhibition generates a host-tumor niche that mediates therapeutic escape. *J Invest Dermatol* 135: 3115–3124
- Flaherty KT, Hodi FS, Fisher DE (2012) From genes to drugs: targeted strategies for melanoma. *Nat Rev Cancer* 12: 349–361
- Fletcher AL, Acton SE, Knoblich K (2015) Lymph node fibroblastic reticular cells in health and disease. *Nat Rev Immunol* 15: 350–361
- Girard CA, Lecacheur M, Ben Jouira R, Berestjuk I, Diazi S, Prod'homme V, Mallavialle A, Larbret F, Gesson M, Schaub S et al (2020) A feed-forward mechanosignaling loop confers resistance to therapies targeting the MAPK pathway in BRAF-mutant melanoma. *Cancer Res* 80: 1927–1941
- Gopal S, Veracini L, Grall D, Butori C, Schaub S, Audebert S, Camoin L, Baudelet E, Radwanska A, Beghelli-de la Forest Divonne S et al (2017) Fibronectin-guided migration of carcinoma collectives. *Nat Commun* 8: 14105
- Grither WR, Longmore GD (2018) Inhibition of tumor-microenvironment interaction and tumor invasion by small-molecule allosteric inhibitor of DDR2 extracellular domain. *Proc Natl Acad Sci USA* 115: E7786–E7794
- Hammerman PS, Sos ML, Ramos AH, Xu C, Dutt A, Zhou W, Brace LE, Woods BA, Lin W, Zhang J et al (2011) Mutations in the DDR2 kinase gene identify a novel therapeutic target in squamous cell lung cancer. *Cancer Discov* 1: 78–89
- Hirata E, Girotti MR, Viros A, Hooper S, Spencer-Dene B, Matsuda M, Larkin J, Marais R, Sahai E (2015) Intravital imaging reveals how BRAF inhibition generates drug-tolerant microenvironments with high integrin β 1/FAK signaling. *Cancer Cell* 27: 574–588
- Hynes RO, Naba A (2012) Overview of the matrisome—an inventory of extracellular matrix constituents and functions. *Cold Spring Harb Perspect Biol* 4: a004903
- Jeitany M, Leroy C, Tosti P, Lafitte M, Le Guet J, Simon V, Bonenfant D, Robert B, Grillet F, Mollevi C et al (2018) Inhibition of DDR1-BCR signalling by nilotinib as a new therapeutic strategy for metastatic colorectal cancer. *EMBO Mol Med* 10: e7918
- Jenkins MH, Croteau W, Mullins DW, Brinckerhoff CE (2015) The BRAF(V600E) inhibitor, PLX4032, increases type I collagen synthesis in melanoma cells. *Matrix Biol* 48: 66–77
- Kalluri R (2016) The biology and function of fibroblasts in cancer. *Nat Rev Cancer* 16: 582–598
- Kaukonen R, Jacquemet G, Hamidi H, Ivaska J (2017) Cell-derived matrices for studying cell proliferation and directional migration in a complex 3D microenvironment. *Nat Protoc* 12: 2376–2390
- Kaukonen R, Mai A, Georgiadou M, Saari M, De Franceschi N, Betz T, Sihto H, Ventelä S, Elo L, Jokitalo E et al (2016) Normal stroma suppresses cancer cell proliferation via mechanosensitive regulation of JMJD1a-mediated transcription. *Nat Commun* 7: 12237
- Kaur A, Webster MR, Marchbank K, Behera R, Ndoye A, Kugel CH, Dang VM, Appleton J, O'Connell MP, Cheng P et al (2016) sFRP2 in the aged microenvironment drives melanoma metastasis and therapy resistance. *Nature* 532: 250–254
- Kim H-G, Tan LI, Weisberg EL, Liu F, Canning P, Choi HG, Ezell SA, Wu H, Zhao Z, Wang J et al (2013) Discovery of a potent and selective DDR1 receptor tyrosine kinase inhibitor. *ACS Chem Biol* 8: 2145–2150
- Kim MH, Kim J, Hong H, Lee SH, Lee JK, Jung E, Kim J (2016) Actin remodeling confers BRAF inhibitor resistance to melanoma cells through YAP/TAZ activation. *EMBO J* 35: 462–478
- Landowski TH, Olashaw NE, Agrawal D, Dalton WS (2003) Cell adhesion-mediated drug resistance (CAM-DR) is associated with activation of NF- κ B (RelB/p50) in myeloma cells. *Oncogene* 22: 2417–2421
- Leitinger B (2014) Discoidin domain receptor functions in physiological and pathological conditions. *Int Rev Cell Mol Biol* 310: 39–87
- Luna A, Elloumi F, Varma S, Wang Y, Rajapakse VN, Aladjem MI, Robert J, Sander C, Pommier Y, Reinhold WC (2021) Cell miner cross-database

- (CellMinerCDB) version 1.2: exploration of patient-derived cancer cell line pharmacogenomics. *Nucleic Acids Res* 49: D1083–D1093
- Meads MB, Gatenby RA, Dalton WS (2009) Environment-mediated drug resistance: a major contributor to minimal residual disease. *Nat Rev Cancer* 9: 665–674
- Misek SA, Appleton KM, Dexheimer TS, Lisabeth EM, Lo RS, Larsen SD, Gallo KA, Neubig RR (2020) Rho-mediated signaling promotes BRAF inhibitor resistance in de-differentiated melanoma cells. *Oncogene* 39: 1466–1483
- Miskolczi Z, Smith MP, Rowling EJ, Ferguson J, Barriuso J, Wellbrock C (2018) Collagen abundance controls melanoma phenotypes through lineage-specific microenvironment sensing. *Oncogene* 37: 3166–3182
- Mondragon L, Mhaidly R, De Donatis GM, Tosolini M, Dao P, Martin AR, Pons C, Chiche J, Jacquin M, Imbert V et al (2019) GAPDH overexpression in the T cell lineage promotes angioimmunoblastic T cell lymphoma through an NF-kappaB-dependent mechanism. *Cancer Cell* 36: 268–287
- Mouw JK, Ou G, Weaver VM (2014) Extracellular matrix assembly: a multiscale deconstruction. *Nat Rev Mol Cell Biol* 15: 771–785
- Müller J, Krijgsman O, Tsoi J, Robert L, Hugo W, Song C, Kong X, Possik PA, Cornelissen-Steijger PDM, Foppen MHG et al (2014) Low MITF/AXL ratio predicts early resistance to multiple targeted drugs in melanoma. *Nat Commun* 5: 5712
- Nadiminty N, Tummala R, Liu C, Yang J, Lou W, Evans CP, Gao AC (2013) NF-kappaB2/p52 induces resistance to enzalutamide in prostate cancer: role of androgen receptor and its variants. *Mol Cancer Ther* 12: 1629–1637
- Nazarian R, Shi H, Wang QI, Kong X, Koya RC, Lee H, Chen Z, Lee M-K, Attar N, Sazegar H et al (2010) Melanomas acquire resistance to B-RAF(V600E) inhibition by RTK or N-RAS upregulation. *Nature* 468: 973–977
- Orgaz JL, Crosas-Molist E, Sadok A, Perdrix-Rosell A, Maiques O, Rodriguez-Hernandez I, Monger JO, Mele S, Georgouli M, Bridgeman V et al (2020) Myosin II Reactivation and Cytoskeletal Remodeling as a Hallmark and a Vulnerability in Melanoma Therapy Resistance. *Cancer Cell* 37: 85–103
- Pickup MW, Mouw JK, Weaver VM (2014) The extracellular matrix modulates the hallmarks of cancer. *EMBO Rep* 15: 1243–1253
- Poudel B, Lee YM, Kim DK (2015) DDR2 inhibition reduces migration and invasion of murine metastatic melanoma cells by suppressing MMP2/9 expression through ERK/NF-kappaB pathway. *Acta Biochim Biophys Sin (Shanghai)* 47: 292–298
- Rambow F, Marine JC, Goding CR (2019) Melanoma plasticity and phenotypic diversity: therapeutic barriers and opportunities. *Genes Dev* 33: 1295–1318
- Rathore M, Girard C, Ohanna M, Tichet M, Ben Jouira R, Garcia E, Larbret F, Gesson M, Audebert S, Lacour JP et al (2019) Cancer cell-derived long pentraxin 3 (PTX3) promotes melanoma migration through a toll-like receptor 4 (TLR4)/NF-kappaB signaling pathway. *Oncogene* 38: 5873–5889
- Reger de Moura C, Battistella M, Sohail A, Caudron A, Feugeas JP, Podgorniak M-P, Pages C, Mazouz Dorval S, Marco O, Menashi S et al (2019) Discoidin domain receptors: a promising target in melanoma. *Pigment Cell Melanoma Res* 32: 697–707
- Rich L, Whittaker P (2005) Collagen and picosirius red staining: a polarized light assessment of fibrillar hue and spatial distribution. *Braz J Morphol Sci* 22: 97–104
- Robert C, Grob JJ, Stroykovskiy D, Karaszewska B, Hauschild A, Levchenko E, Chiarion Sileni V, Schachter J, Garbe C, Bondarenko I et al (2019) Five-year outcomes with dabrafenib plus trametinib in metastatic melanoma. *N Engl J Med* 381: 626–636
- Robert G, Gaggioli C, Bailet O, Chavey C, Abbe P, Aberdam E, Sabatié E, Cano A, Garcia de Herreros A, Ballotti R et al (2006) SPARC represses E-cadherin and induces mesenchymal transition during melanoma development. *Cancer Res* 66: 7516–7523
- Seguin L, Desgrosellier JS, Weis SM, Cheresh DA (2015) Integrins and cancer: regulators of cancer stemness, metastasis, and drug resistance. *Trends Cell Biol* 25: 234–240
- Sero JE, Sailem HZ, Ardy RC, Almuttaqi H, Zhang T, Bakal C (2015) Cell shape and the microenvironment regulate nuclear translocation of NF-kappaB in breast epithelial and tumor cells. *Mol Syst Biol* 11: 790
- Shain AH, Bastian BC (2016) From melanocytes to melanomas. *Nat Rev Cancer* 16: 345–358
- Shrivastava A, Radziejewski C, Campbell E, Kovac L, McGlynn M, Ryan TE, Davis S, Goldfarb MP, Glass DJ, Lemke G et al (1997) An orphan receptor tyrosine kinase family whose members serve as nonintegrin collagen receptors. *Mol Cell* 1: 25–34
- Smith MP, Brunton H, Rowling EJ, Ferguson J, Arozarena I, Miskolczi Z, Lee JL, Girotti MR, Marais R, Levesque MP et al (2016) Inhibiting drivers of non-mutational drug tolerance is a salvage strategy for targeted melanoma therapy. *Cancer Cell* 29: 270–284
- Straussman R, Morikawa T, Shee K, Barzily-Rokni M, Qian ZR, Du J, Davis A, Mongare MM, Gould J, Frederick DT et al (2012) Tumour microenvironment elicits innate resistance to RAF inhibitors through HGF secretion. *Nature* 487: 500–504
- Taniguchi K, Karin M (2018) NF-kappaB, inflammation, immunity and cancer: coming of age. *Nat Rev Immunol* 18: 309–324
- Tichet M, Prod'Homme V, Fenouille N, Ambrosetti D, Mallavialle A, Cerezo M, Ohanna M, Audebert S, Rocchi S, Giaccherio D et al (2015) Tumour-derived SPARC drives vascular permeability and extravasation through endothelial VCAM1 signalling to promote metastasis. *Nat Commun* 6: 6993
- Tsoi J, Robert L, Paraiso K, Galvan C, Sheu KM, Lay J, Wong DJL, Atefi M, Shirazi R, Wang X et al (2018) Multi-stage Differentiation Defines Melanoma Subtypes with Differential Vulnerability to Drug-Induced Iron-Dependent Oxidative Stress. *Cancer Cell* 33: 890–904
- Tu MM, Lee FYF, Jones RT, Kimball AK, Saravia E, Graziano RF, Coleman B, Menard K, Yan J, Michaud E et al (2019) Targeting DDR2 enhances tumor response to anti-PD-1 immunotherapy. *Sci Adv* 5: eaav2437
- Valiathan RR, Marco M, Leitinger B, Kleer CG, Fridman R (2012) Discoidin domain receptor tyrosine kinases: new players in cancer progression. *Cancer Metastasis Rev* 31: 295–321
- Verfaillie A, Imrichova H, Atak ZK, Dewaele M, Rambow F, Hulselmans G, Christiaens V, Svetlichnyy D, Luciani F, Van den Mooter L et al (2015) Decoding the regulatory landscape of melanoma reveals TEADS as regulators of the invasive cell state. *Nat Commun* 6: 6683
- Vogel W, Gish GD, Alves F, Pawson T (1997) The discoidin domain receptor tyrosine kinases are activated by collagen. *Mol Cell* 1: 13–23
- von Mässenhausen A, Sanders C, Brägelmann J, Konantz M, Queisser A, Vogel W, Kristiansen G, Duensing S, Schröck A, Bootz F et al (2016) Targeting DDR2 in head and neck squamous cell carcinoma with dasatinib. *Int J Cancer* 139: 2359–2369
- Widmer DS, Cheng PF, Eichhoff OM, Belloni BC, Zipser MC, Schlegel NC, Javelaud D, Mauviel A, Dummer R, Hoek KS (2012) Systematic classification of melanoma cells by phenotype-specific gene expression mapping. *Pigment Cell Melanoma Res* 25: 343–353
- Wouters J, Kalender-Atak Z, Minnoye L, Spanier KI, De Waegeneer M, Bravo González-Blas C, Mauduit D, Davie K, Hulselmans G, Najem A et al (2020) Robust gene expression programs underlie recurrent cell

states and phenotype switching in melanoma. *Nat Cell Biol* 22: 986–998

Yeung DA, Shanker N, Sohail A, Weiss BA, Wang C, Wellmerling J, Das S, Ganju RK, Miller JLC, Herr AB *et al* (2019) Clustering, spatial distribution, and phosphorylation of discoidin domain receptors 1 and 2 in response to soluble collagen I. *J Mol Biol* 431: 368–390

Young HL, Rowling EJ, Bugatti M, Giurisato E, Luheshi N, Arozarena I, Acosta J-C, Kamarashev J, Frederick DT, Cooper ZA *et al* (2017) An adaptive

signaling network in melanoma inflammatory niches confers tolerance to MAPK signaling inhibition. *J Exp Med* 214: 1691–1710



License: This is an open access article under the terms of the Creative Commons Attribution License, which permits use, distribution and reproduction in any medium, provided the original work is properly cited.